Cell Reports
Methods

Article

Revealing viral and cellular dynamics of HIV-1 at the single-cell level during early treatment periods

Graphical abstract

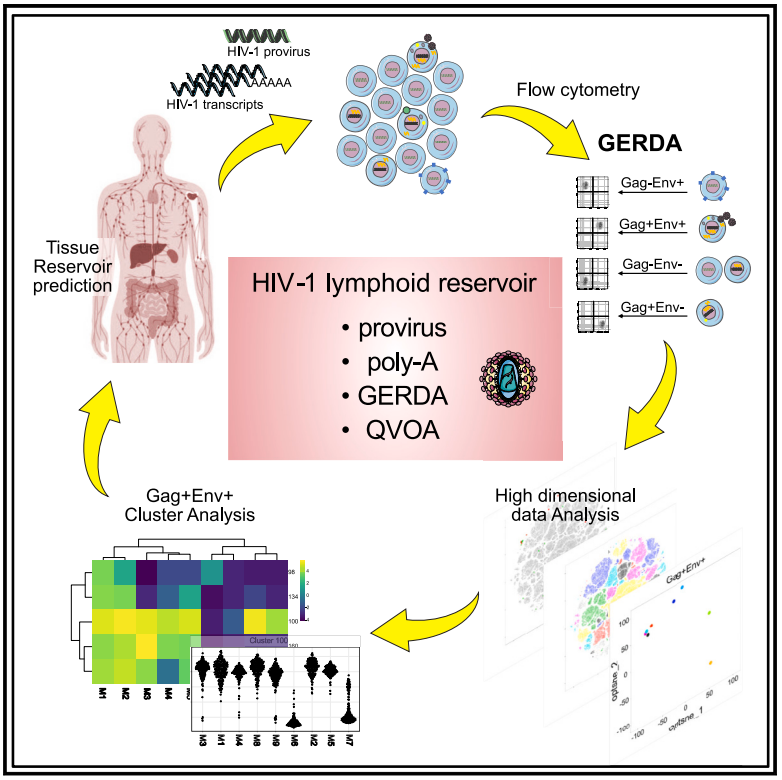

Highlights

- GERDA is a method to decipher the HIV-1 tissue contribution using peripheral blood
- Sensitive detection down to 1 cell per million targeting different splice products
- HIV-1 stays transcriptionally active even during viral suppression by ART
- The replicating HIV-1 reservoir resides mainly in naive and central memory T cells

Authors

Fabian Otte, Yuepeng Zhang, Julian Spagnuolo, ..., Karin J. Metzner, Thomas Klimkait, the Swiss HIV Cohort Study

Correspondence

fabian.otte@unibas.ch (F.O.), thomas.klimkait@unibas.ch (T.K.)

In brief

Unraveling the true functional HIV-1 reservoir is challenging since ≥95% of integrated viruses are defective. Here, Otte et al. present an approach that integrates multiple markers to sensitively detect the functional cellular HIV-1 blood reservoir early after diagnosis and to predict the intact viral reservoir in peripheral tissues.

Otte et al., 2023, Cell Reports Methods 3, 100485
June 26, 2023
https://doi.org/10.1016/j.crmeth.2023.100485

CellPress

Cell Reports Methods

CellPress
OPEN ACCESS

Article

Revealing viral and cellular dynamics of HIV-1 at the single-cell level during early treatment periods

Fabian Otte,[1,8,*] Yuepeng Zhang,[1,8] Julian Spagnuolo,[2] Alexander Thielen,[3] Martin Däumer,[3] Carsten Wiethe,[4] Marcel Stoeckle,[5] Katharina Kusejko,[6] Florian Klein,[7] Karin J. Metzner,[6] Thomas Klimkait,[1,9,*] and the Swiss HIV Cohort Study

[1]Molecular Virology, Department Biomedicine, University of Basel, 4009 Basel, Switzerland
[2]Experimental Immunology, Department Biomedicine, University of Basel, 4056 Basel, Switzerland
[3]Seq-IT GmbH & Co.KG, 67655 Kaiserslautern, Germany
[4]Biolegend GmbH, 56070 Koblenz, Germany
[5]Infectiology, University Hospital Basel, 4031 Basel, Switzerland
[6]Division of Infectious Diseases and Hospital Epidemiology, University Hospital Zurich, and Institute of Medical Virology, University of Zurich, 8091 Zurich, Switzerland
[7]Laboratory of Experimental Immunology, Institute of Virology, Faculty of Medicine and University Hospital Cologne, University of Cologne, 50931 Cologne, Germany
[8]These authors contributed equally
[9]Lead contact
*Correspondence: fabian.otte@unibas.ch (F.O.), thomas.klimkait@unibas.ch (T.K.)
https://doi.org/10.1016/j.crmeth.2023.100485

MOTIVATION HIV-1 monitoring mainly focuses on clinical manifestation and immunological deterioration, and cell-type-specific viral activity is often not discernible. Most current HIV-1 quantification assays use HIV-1 DNA, RNA, Gag protein, or progeny virus, often leading to a significant over- or underestimation of the viral reservoir.

We propose an approach for identification and characterization of cellular reservoirs that takes into account cellular tissue-homing properties and the combined expression of predictive viral proteins, i.e., Gag and Env, by fluorescence-activated cell sorting (FACS) of cells in the circulating blood. Venipuncture, rather than biopsies, allows a short handling time and low sample consumption. This method combines favorable sensitivity and specificity and enables robust tissue reservoir prediction.

SUMMARY

While combination therapy completely suppresses HIV-1 replication in blood, functional virus persists in $CD4^+$ T cell subsets in non-peripheral compartments that are not easily accessible. To fill this gap, we investigated tissue-homing properties of cells that transiently appear in the circulating blood. Through cell separation and *in vitro* stimulation, the HIV-1 "Gag and Envelope reactivation co-detection assay" (GERDA) enables sensitive detection of Gag+/Env+ protein-expressing cells down to about one cell per million using flow cytometry. By associating GERDA with proviral DNA and polyA-RNA transcripts, we corroborate the presence and functionality of HIV-1 in critical body compartments utilizing t-distributed stochastic neighbor embedding (tSNE) and density-based spatial clustering of applications with noise (DBSCAN) clustering with low viral activity in circulating cells early after diagnosis. We demonstrate transcriptional HIV-1 reactivation at any time, potentially giving rise to intact, infectious particles. With single-cell level resolution, GERDA attributes virus production to lymph-node-homing cells with central memory T cells (T_{CM}s) as main players, critical for HIV-1 reservoir eradication.

INTRODUCTION

HIV-1 infects $CD4^+$ cells using either CCR5 or CXCR4 for entry. After primary HIV-1 infection, a founding population of viruses and virus-infected cells is rapidly established and expanded in various body compartments. The proviral landscape is dynamically shaped over time by key contributors such as cell elimination,[1,2] clonal expansion of HIV-1-harboring cells,[3,4]

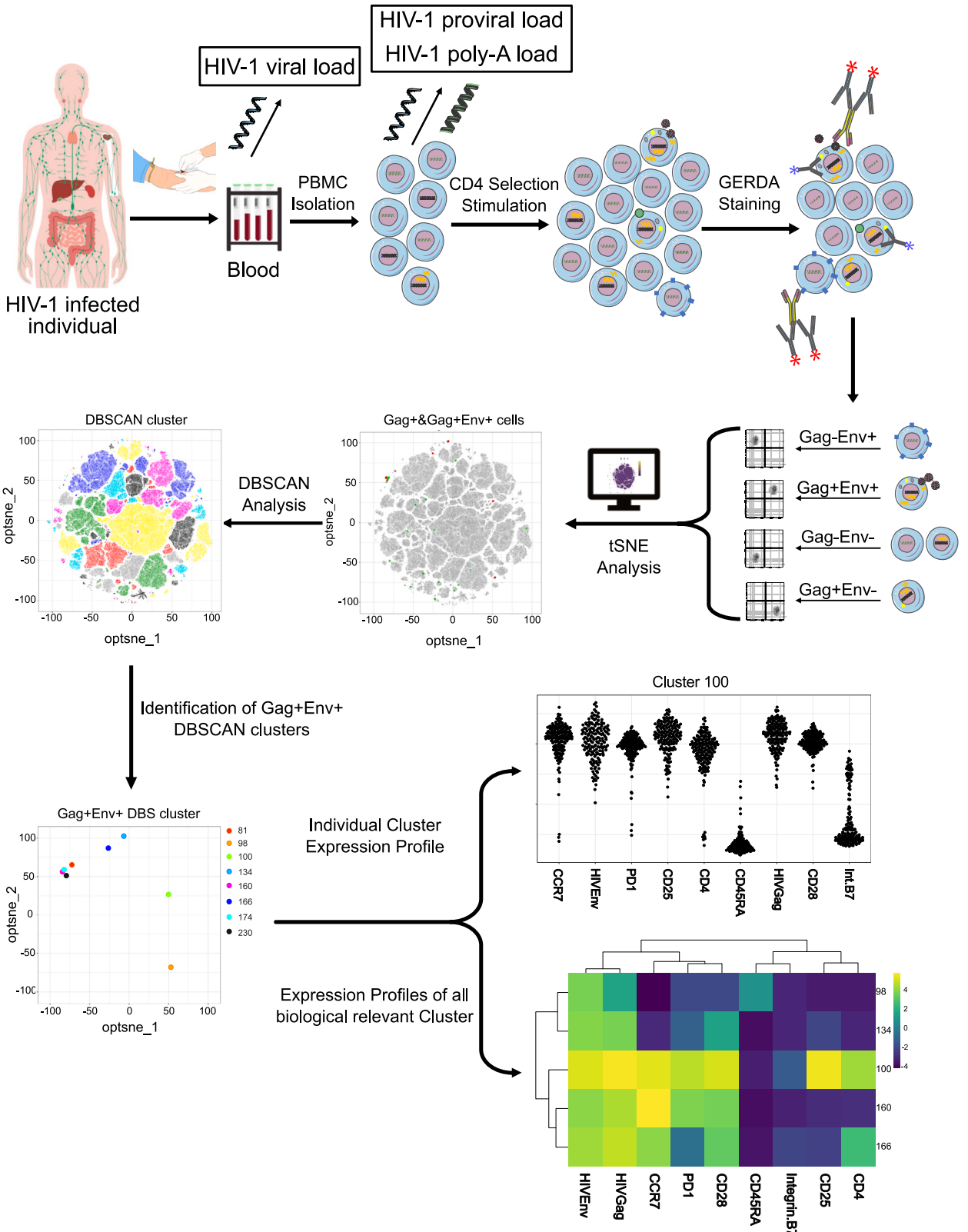

(legend on next page)

homeostatic[5–7] or antigenic proliferation,[8,9] leading to a continuous modulation and adaptation, while antiretroviral therapy (ART) sustains pressure on the virus.

ART completely suppresses viral replication in peripheral blood. Consequently, after entering a controlled, chronic phase of HIV-1 infection, the main viral reservoir of intact proviral genomes is expected to reside in memory T cell subsets that persist for years.[10–12] Therefore, infected cells are found mainly in various distant organs, including lymph nodes, gut, brain, and others.[13,14]

Multiple approaches to quantitatively reactivate latent proviruses during suppressive ART have failed or were only marginally successful.[15] In contrast, even after extended periods of complete viral suppression, a therapy interruption typically induces the rapid rebound of HIV-1 in peripheral blood.[13]

Transiently circulating T cells in the peripheral blood mononuclear cell (PBMCs) pool are, from a clinical perspective, highly attractive and can be easily obtained by venipuncture. In these blood cell preparations, organ-specific non-peripheral cells with tissue-homing markers can also transiently appear.[16–20] As a consequence, any PBMC preparation, e.g., from EDTA blood or cell preparation tubes, is expected to contain such non-peripheral cells. And, if viral replication properties principally differ in those tissue-derived leukocytes, the accidental co-isolation could lead to false interpretations.

In order to specifically interrogate the role of transiently appearing non-peripheral cells, this study aimed at separating and characterizing leukocytes with external homing properties using characteristic homing markers such as integrin $\alpha_4\beta_7$ for gut homing[16,17] and cutaneous leukocyte antigen (CLA) for skin homing,[21] as well as CCR7 for lymph node homing.[19] We obtained peripheral blood and employed labeling and preparation methods that permit the selective harvest of cells with known surface markers.

For assessing whether tissue markers correlate with "the true" functional HIV-1 reservoir *in vivo*—i.e., cell population(s) that are responsible for the viral rebound after therapy cessation—a plethora of assays that detect HIV-1 DNA or RNA, viral proteins, or extracellular (EC) viral products after viral outgrowth have been described.[22–26] Also, the monocytic marker CD32a is among the biomarkers linked to HIV-1 reservoirs,[27] but this information is still being disputed.[28–30] Yet, one key limitation of most systems is that during therapy $\geq$95% of all detected integrated proviral genomes are defective.[31,32] Typically, defects are characterized by genomic deletions or APOBEC-mediated hypermutations, which still leave many viral genomes capable of producing isolated viral transcripts and proteins[33–35] and leading to positive RNA signals, which might erroneously suggest intact genomes in a given HIV-1 reservoir.

The approach described here, termed GERDA (Gag and Envelope reactivation co-detection assay), uses HIV-1 Gag protein expression as a first proxy for viral activity and ensures that arising particles are associated with the HIV-1 Envelope protein. For the latter, and to minimize the effects of natural mutations occurring in the Envelope (Env) protein, the use of specific broadly neutralizing antibodies (bNAbs) is utilized. GERDA aims at a sensitive characterization of virus-releasing cells and the functional analysis of virions.

Our study demonstrates the validity and favorable features of GERDA as being comparable or superior to other sensitive reservoir assays. Moreover, GERDA is able to characterize the Gag+/Env+ translation-competent cell population(s) during early therapy at a single-cell level.

RESULTS

Simultaneous detection of HIV-1 Gag and Env proteins on HIV-1-infected cells

Specialized methods for characterizing tissue reservoirs of HIV-1 rely on biopsy material from the organ of interest and often rely on cell-associated viral transcripts or the Gag p24 protein. Many of these assays lack the ability to exclude defective proviruses.

We therefore set out to establish a method that captures the entire infectious reservoir by linking intracellular (IC) HIV-1 Gag expression and EC HIV-1 Env presentation. To identify productively infected T cells, our approach utilizes the combined detection of Gag and Env proteins: Gag serves a proxy for the production of viral particle components, while Env indicates the presence of the essential viral receptor-binding function for the target cell. Thereby, the combination covers the functionality of most of the viral genome length, thus avoiding a 5′ or 3′ constrained bias (of note, 70%–83% of defective proviruses correlate with the presence of extended deletions[36,37]). Additionally, it detects proteins translated from different HIV-1 mRNA splice products. Figure 1 highlights the workflow, requiring only small sample volumes of $\leq$40 mL whole blood and being completed within 9 h of hands-on time, which favorably compares with other flow cytometry techniques.[24,38–40] Semi-automated computational analysis allows us to process all data in a standardized way to have the same treatment of all data points.

To validate the procedure, we first demonstrated that each cell type in a defined mix of HIV-1-positive (HIV-1+) and -uninfected cells can be identified. For this, chronically infected HUT4-3[41] and uninfected SupT1 cells were mixed at predefined ratios and stained for HIV-1 Gag, HIV-1 Env (HUT4-3), and CD4 (expressed by SupT1) (Figures S1A, S1B, and S1D–S1G). As shown in Figure 2A, HIV-infected cells localize as one distinct, Gag+/Env+ double-positive population with a tight correlation of both parameters (R^2 = 0.66, $p < 2.2 \times 10^{-16}$; Figure S1C), clearly separating them from uninfected SupT1 cells.

Figure 1. Workflow of GERDA for simultaneous detection of HIV-1 Gag and Env proteins on HIV-1 infected cells

Venous blood is drawn from HIV+ individuals. Blood is separated into cell-free plasma for viral load determination and the PBMC fraction for proviral and poly-A transcript load. Preselected CD4 untouched PBMCs, PHA stimulated, are labeled for immunological markers HIV-1 Env (antibody: red asterisks), and intracellularly for HIV-1 Gag (antibody: blue asterisks). Various cellular HIV-1 reservoirs are analyzed for HIV-1 Env and HIV-1 Gag to assess a contribution to the viral reservoir using dimensional reduction and cluster analysis of acquired FACS data by tSNE and DBSCAN. Gag- (green) and Env- (red)expressing cells are identified on tSNE plots and further refined by DBSCAN clustering (the represented color palette cannot highlight each individual cluster). HIV-1 Gag+/Env+ clusters identified by DBSACN were either analyzed by Beeplot for individual cell staining events or as heatmap as mean expression for each cluster.

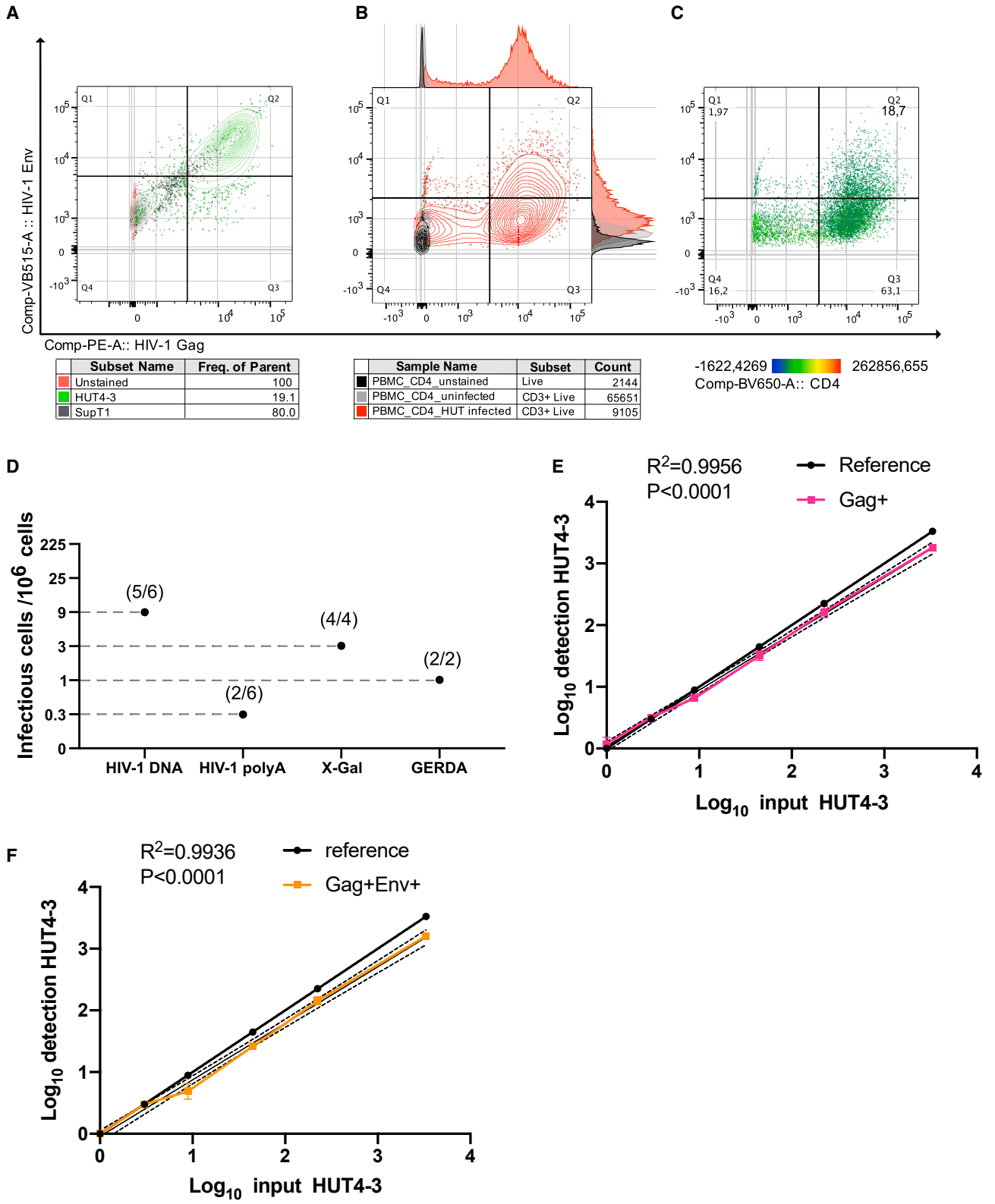

Figure 2. Specificity and sensitivity of GERDA

(A) HIV-1 Gag+/Env+ staining on a mixed pool of infected (HUT4-3: green) and uninfected (SupT1: gray) cells. Unstained mix in red.

(B) HIV-1 Gag+/Env+ staining of infected CD4$^+$ T cells (red) and unstained (black) and uninfected (light gray) controls.

(legend continued on next page)

Then, uninfected PBMCs or SupT1 cells were PHA (phytohaemagglutinin) stimulated, to increase the infection potential, and were used for cell-free infection with several laboratory strains of HIV-1, covering two HIV-1 subtypes and tropisms (subtype B: HIV-1NL4-3, HIV-1LAI, HIV-1Ala; all X4 tropic; subtype D: HIV-1Mal; R-5 tropic). After extensive washing and the 3 day infection period, cells (for GERDA) and supernatant (containing cell-derived virus to assess infectivity) were used to verify that Gag+/Env+ double-positive cells are indeed able to initiate a productive virus infection via a co-cultivation with the long terminal repeat (LTR)-dependent lacZ indicator cells SX-R5.[42] As illustrated in Figure 2B (and Figure S1D), infections of either cell type yielded Gag+/Env+ positive cells, that gave rise to infectious progeny virus confirmed by semi-quantitative X-Gal stainings (exemplified in Figures S1J and S1K). X-Gal staining and, depending on the HIV-1 tropism, syncytia formation proved the presence of intact, infectious virus particles (Figures S1J, S1K, S2C, and S5C). Of note and as expected, while CD4 expression became downmodulated in all Gag+/Env+ double-positive cells, it remained high in the uninfected control cells (Figures 1D, S1E, S1G, S1I, and S1M). In our hands, the SXR5 system yielded clearer infection events, while overall, the sensitivity correlated very well with the TZM-bl cells[43] used by others (Figures S1J and S1K). For evaluating assay linearity and specificity, a defined number of infected HUT4-3 cells were spiked into Ramos cells, which cannot be infected with HIV-1. This avoided the initiation of infection events from infectious HUT4-3 cells. For titration, quantities of 100,000, 2,250, 225, 45, 9, 3, 1, or 0.3 presumed infectious HUT4-3 cells were spiked for a total number of 10^6 cells. We benchmarked the GERDA assay throughout all molecular levels by determining HIV-1 DNA load and the poly-A transcript load as well as the free infectious virus by determining the detection limit of each assay in aliquots from each titration step (Figure 2D). Staining demonstrated a very consistent detection down to about 1 copy, shown in Figures 2E and 2F (Gag+ detected 1/1 × 10^6, $R^2 = 0.9956$, $p < 0.0001$; Gag+/Env+ detected 1/1 × 10^6, $R^2 = 0.9936$, $p < 0.0001$), which is in good agreement with all other assays tested in benchmarking experiments and confirmed the high sensitivity of the GERDA system. Backgating revealed that HUT4-3 is readily detected when titrations (Figure S2D) were compared with control stains of HUT4-3 only (Figure S2E). No unspecific staining of Ramos cells was observed (Figure S2F), further supporting the high HIV-1 specificity of the GERDA system.

Immune characterization of recently diagnosed patients with HIV-1

It is known that cells circulating in the peripheral blood are not at all a homogeneous population of PBMCs but that they can also stem from distant compartments and immunological organs and only transiently appear in circulating blood. It is therefore likely that such different cell homing also associates with distinct viral properties, as viral activity and sequence stability can vary significantly for the different compartments.[13,14,44,45] To determine the origin of cells as putative viral reservoirs that appear in peripheral blood, we used the molecular identity of infected cells via viral and lymphoid homing markers. For the analysis of the very complex multidimension dataset, t-distributed stochastic neighborhood embedding (tSNE)[46] and density-based spatial clustering of applications with noise (DBSCAN)[47] were applied. The tSNE tool was established for the graphical presentation of high-dimensional data using algorithms to reduce dimensionality to 2–3 dimensions. tSNE clusters cells with very similar properties in close proximity to each other in tSNE space. For cluster analysis with higher resolution, DBSCAN was employed, identifying small clusters of down to 5 cells with similar expression profiles, which we considered critical for very small or diverse HIV-1 cell reservoirs. DBSCAN works in tSNE space using its 2 parameters—"minimal points," representing minimal numbers of cells to form a cluster, and "epsilon," the maximal tSNE distance individual data points of one cluster can have.

As various T cell subsets are the main contributors to the persisting HIV-1 pool during therapy, we used cryo-preserved PBMCs, which had been obtained prior to ART initiation from individuals infected with HIV-1 within the Swiss HIV cohort study (SHCS). Uninfected cells (Figure S3A) served as references to set Gag+/Env+ thresholds. Because cell counts in cryo-preserved specimens were rather low, and since individual properties were considered irrelevant for this validation, PBMC samples from four SHCS individuals before ART initiation[48,49] with high proviral loads ($\geq 1 \times 10^4$ per million cells) were pooled. We assumed that a high viral DNA content would be suggestive of high viral activity in the respective samples. As illustrated in Figure 3A, the overall infection rates with about 70 infected cells per 10^6 $CD3^+$ viable CD4 T cells in this cell pool were low with a decent, significant correlation of Gag+/Env+ double-positive expression signals ($R^2 = 0.34$, $p = 0.017$; Figure S3B). Rare double-positive event contribution to total CD4 cell pool was clustered and identified by tSNE and DBSCAN (Figures S3C–S3E). Marker profiles of biologically relevant identified clusters are summarized in the heatmap in Figure S3F. DBSCAN identified double-positive clusters with distinct differentiation statuses (cluster 367: central memory T cells [T_{CM}s]; clusters 104, 206, and 237: naive T cells [T_Ns]; cluster 154: terminally differentiated effector memory T cells [T_{EMRA}s]), differential CD4 expression levels, a higher degree of exhaustion (PD1+), and variable gut-homing potential (integrin β_7+). This finding was well in line with classical gating (Figure S3G). Regarding homing markers, CCR7+ cells were mainly found in double-positive events representing T_N or T_{CM} T cell subsets.

For the study of various representative infection situations, a sufficient sample of viable T cells in ca. 40 mL fresh blood from recently diagnosed, consenting individuals was obtained. We anticipated a higher proportion of circulating, productively infected cells in the group of eight study participants, who were chosen to

(C) CD4 expression heatmap of $CD4^+$ T cells infected with HUT4-3 virus. Rainbow color map for low (blue) to high (red) expression level of CD4 at the bottom.
(D) Detection limit of all HIV-1 reservoir detection assays next to GERDA. Gray dotted line highlights detection limits of each assay. Numbers in brackets show number of positive replicates at the lowest positively tested titration step.
(E and F) Input of infectious cell vs. cells actually detected for HIV-1 Gag+ (E) or Gag+/Env+ cells at each titration step. Theoretical detection limit in black. Fitted curves with mean and SD for Gag+ (magenta) and Gag+/Env+ (orange) are given with respective R^2 and p values. Light gray lines delineate confidence intervals.

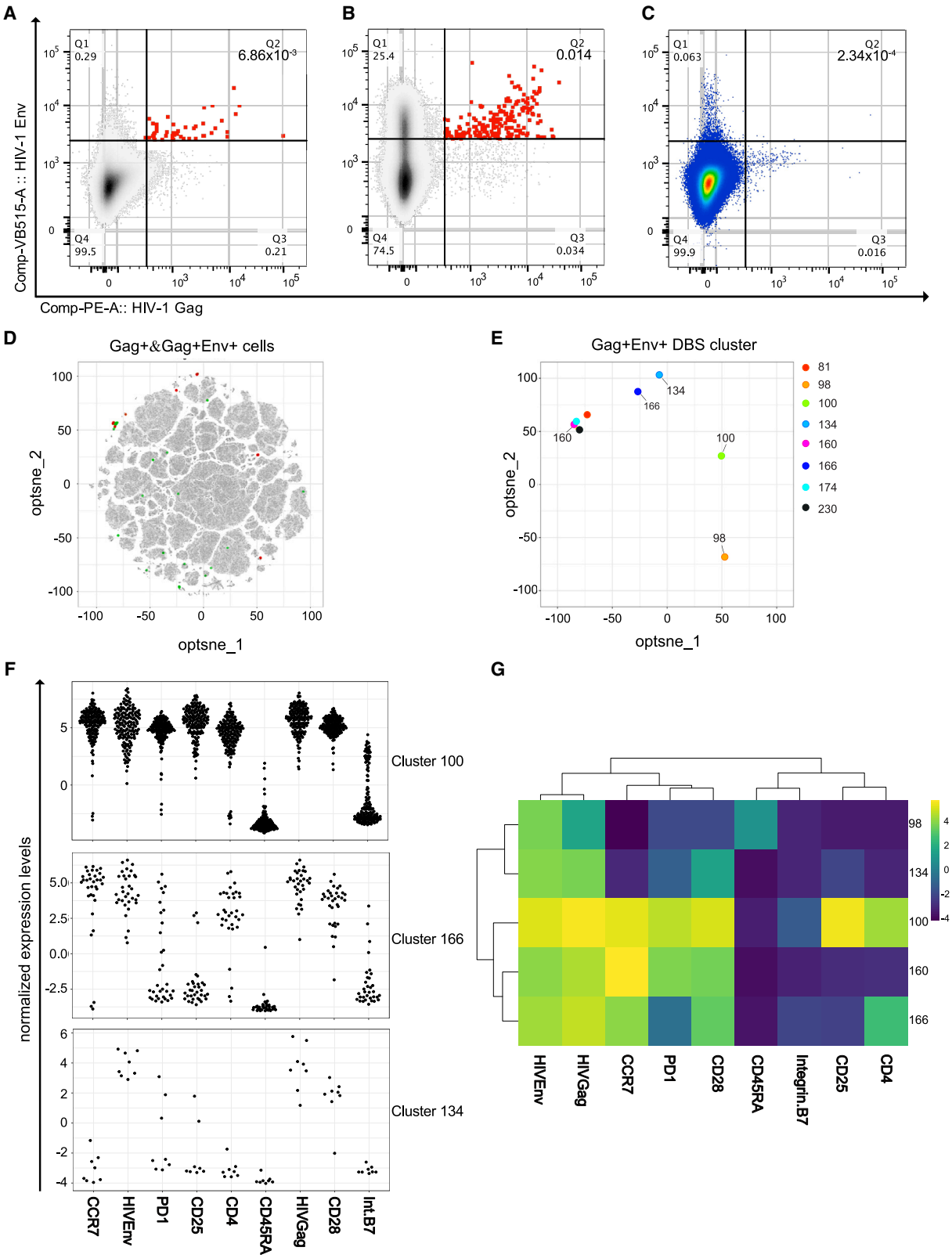

(legend on next page)

represent "typical infection situations" with HIV-1 and covering acute infection, various stages at the time of treatment initiation, and late presentation without therapy (Figures S1 and S2; Table 1).

- For n = 3 individuals, infections were classified "early," with a first positive HIV-1 test less than 1 year ago (P01_46, P02_53, P03_61), and P02_53 was at a very early stage of Fiebig stage II.
- CD4 counts were between 322 and 1,928/mm^3 blood for n = 6 (P01_46, P02_53, P03_61, P05_66, P07_07, and P08_45), with %CD4 over 30% for n = 2 (P02_53 and P07_07).
- Samples from all individuals except P07_07 (n = 7) were taken at treatment initiation or just before. Prior to first sampling, P06_67 had experienced a viral load (VL) relapse with a VL >500,000 copies/mL (c/mL) and very low CD4. For six individuals, a follow-up period of 127–811 days was covered in this study. For P08_45, only a single sample was available, and P06_67 was followed during the 39 days of the initial VL decline.

Included individuals were all suppressed within short period of time and stayed suppressed.

While for all individuals, RNA VL was positive at study start (except for P07_07) and HIV-1 DNA remained detectable in peripheral blood during the entire observation period, cell-associated Gag+/Env+ protein double-positive events were much rarer in the samples (median 13.5/1 × 10^6 CD3$^+$ viable CD4 T cells;Figures S4A–S4G; Table 1). 4/7 cases with VLs between 90 and 51,000 copies/mL had no viral activity inside circulating cells based on transcriptional (HIV-1 poly-A) and translational (GERDA) levels. Late presenters, especially P04_56 and P06_67, consistently presented a higher percentage of double-positive cells but also 20%–50% Gag single positives. Of note, this high percentage of single-positive events refers to the amount in the subfraction of cells after CD4 selection, while the overall number of CD4$^+$ cells/leukocytes was rather low. Proviral loads were very low, and no poly-A transcripts were detected just looking at bulk PBMCs, while patients had a low percentage of CD4$^+$ leukocytes (both 6%, 123 or 53 CD4/μL, respectively).

Despite the very low level of Gag+/Env+ double-positive cells for patient P04_56 during periods of VL suppression, the reappearance of viral poly-A transcripts highlights that even under suppressive ART, viral reactivation can occur in certain cell compartments (Table 1).

In this small but representative cohort, individual P01_46 presented with the highest proviral load (4,412 copies/1 × 10^6 cells) and the highest level of HIV-1 poly-A+ transcripts (85,033 copies/1 × 10^6 cells) (Table 1), and these correlated with the high number of Gag+ (480/1 × 10^6 CD3$^+$ viable CD4 T cells) and Gag+/Env+ double-positive cells (140/1 × 10^6 CD3$^+$ viable CD4 T cells), as shown in Figure 3B. The double-positive cell signals thereby closely correlate for both markers (R^2 = 0.44, p = 0.14 × 10^{-11}; Figure S3H). For most individuals, sampling started with detectable VLs between 7,800 and 556,000. During the course of the study, most individuals experienced good VL control to below 100 c/mL (Table 1).

For the analysis of T cells, dimension reduction and unsupervised clustering (Figures 3D, 3E, and S3I) revealed that the highest T cell contribution stemmed from T_{CM} pools of individual P01_46 (Figures 3F and 3G, clusters 100, 160, and 166) as the main viral reservoir in this individual: the typical Gag+/Env+ population was CD4$^+$ and had high levels of cell exhaustion (PD1+), high levels of lymph node (LN)-homing potential (CCR7+), and no or very little gut-homing potential (integrin β_7+).

For individuals at very early time points after infection, a rapid decline over time of viral activity after combination ART (cART) initiation was corroborated, exemplified for the viral and provirus profiles of individual P01_46, after analysis by GERDA (HIV-1 Gag+/Env+ 2/1 × 10^6 CD3$^+$CD4$^+$ cells), proviral load (1,297/1 × 10^6 PBMCs), and HIV-1 transcription (418/1 × 10^6 PBMCs) (Figure 3C; Table 1).

In summary, it might be expected that at very early sampling dates, viral activity would be particularly high and correlate with the high plasma VLs in peripheral blood as observed at these time points. In contrast, we consistently observed that inside the cells of all patients in the study, HIV-1 DNA and poly-A transcripts as well as Gag+/Env+ translation competence, were always low. This correlates with the reported only slow establishment of a persistent viral reservoir in distant target tissues.

GERDA performance during viral outgrowth

To relate the reliable, sensitive detection of viral activity by GERDA to the outgrowth of infectious virus, the Gag+/Env+ test format was compared with viral infection using a published sensitive LTR-induction assay.[42] Peripheral leukocytes from individuals infected with HIV 6 months after diagnosis were CD4-preselected and sorted into their respective memory compartments to separate cells of different origin and to retain the cellular phenotype at time of harvest (Figure S5A). The cell fractions were then stimulated with an antibody cocktail directed against CD3, CD28, and CD2 that resembles the physiological activation of T cells to reactivate putative latent viral genomes. After 14 days of cultural expansion, GERDA and quantitative viral outgrowth assay (QVOA) were performed side by side. We chose several typical, clinically relevant situations during the HIV-1 infection course.

The first situation, clinical sample P01_46, stemmed from an individual with a history of a recent HIV-1 infection who presented

Figure 3. GERDA staining of PBMCs of individuals infected with HIV-1 with CD4 preselected cells, pregated on CD3$^+$CD19$^-$CD8$^-$ viable cells

(A and B) Gag vs. Env expression of cryo-preserved PBMCs before ART initiation (A) or from one recently diagnosed ART-naive individual (P01_46) (B). Double-positive-stained cells in red.

(C) Gag vs. Env expression on day 53 in individual P01_46.

(D and E) tSNE plots of first time point of individual P01_46 (Figure 2B). Each dot represents one cell as a single data point (1.41 × 10^6 cells in total). Gag+ (green) and Gag+/Env+ (red) populations (D) and DBSCAN clusters of Gag+/Env+ cells (E) are shown.

(F) Individual cell marker expression profiles of the representative cluster identified in (E) by DBSCAN.

(G) Marker expression heatmap of all identified biologically relevant clusters; examined markers as x axis, and y axis as cluster IDs. Scale indicates heatmap gradient color of low (purple) to high (yellow) marker expression.

Table 1. Summary table of Patient-related clinical data

Patient ID	Time point	Days since ART start	RNA VL (copies/mL)	CD4 (cells per μL)/% $CD4^+$ lymphocytes	HIV-1 DNA/10^6 PBMCs	HIV-1 DNA/10^6 CD4	HIV-1 poly-A/10^6 PBMCs	HIV-1 poly-A/HIV-1 DNA	GERDA Gag+/Env+ events (%)	Recency/history
P01_46	TP0	−11	867,496	N/A	N/A	N/A	N/A	N/A	N/A	1st year of infection
	TP1	0	143,033	511/16%	4,414	27,588	85,033	19.26	204 (0.014)	
	TP2	17	2,553	N/A	3,743	N/A	N/A	–	N/A	
	TP3	52	142	807/32%	1,297	4,053	418	0.32	4 (2.34×10^{-4})	
	TP4	168	84	761/40%	531	1,328	N/D	N/D	N/A	
	TP5	296	0	N/A	347	N/A	N/D	N/D	N/A	
P2-53	TP0	−1	28,427	1,310/40%	N/A	N/A	N/A	N/A	N/A	acute infection
	TP1	12	90	1,928/50%	276	552	N/D	N/D	3 (1.8×10^{-4})	
	TP2	39	0	1,224/42%	229	545	N/D	N/D	9 (5.24×10^{-4})	
	TP3	139	0	1,901/43%	92	214	N/A	N/A	N/A	
	TP4	241	0	1,259/38%	43	113	N/A	N/A	N/A	
P03_61	TP0	−9	113,370	599/23%	N/A	N/A	N/A	N/A	N/A	1st year of infection
	TP1	0	50,666	472/21%	99	471	N/D	N/D	3 (6.43×10^{-4})	
	TP2	21	N/A	N/A	41	N/A	N/A	N/A	0	
P04-56	TP0	0	43,064	65/4%	2,559	63,975	22,631	8.84	N/A	late presenter
	TP1	8	N/A	N/A	65	N/A	N/D	N/D	6 (0.041)	
	TP2	14	150	N/A	N/A	N/A	N/A	N/A	N/A	
	TP3	55	0	123/6%	1,983	33,050	N/D	N/D	19 (0.057)	
	TP4	170	0	103/8%	1,275	15,938	1,129	0.89	N/A	
	TP5	261	0	110/7%	1,270	18,142	N/A	N/A	N/A	
P05_66	TP0	−21	7,670	433/26%	N/A	N/A	N/A	N/A	N/A	established infection (inf. date unknown)
	TP1	−15	4,808	322/25%	20	80	N/D	N/D	5 (1.78×10^{-3})	
	TP2	1	N/A	N/A	2,562	N/A	N/A	N/A	4 (2.02×10^{-2})	
	TP3	14	0	N/A	33	N/A	N/D	N/D	N/A	
	TP4	127	0	630/27%	13	46	N/D	N/D	N/A	
P06_67	TP0	0[a] (6,604)[b]	555,625	20/4%	N/A	N/A	N/A	N/A	N/A	late presenter (TP0 VL relapse)
	TP1	12[a] (6,616)[b]	9,450	53/6%	1,074	17,900	1,628	1.52	19 (0.21)	
	TP2	39[a] (6,643)[b]	200	N/A	820	N/A	4,368	5.33	10 (8.7×10^{-4})	
P07_07	TP1	531	0	506/32%	N/D	N/D	N/D	N/D	0	> 1 year, delayed sampling
	TP2	629	N/A	N/A	50	N/A	N/A	N/A	0	
	TP3	713	0	513/27%	18	67	N/A	N/A	N/A	
	TP4	811	N/A	N/A	5	N/A	N/D	N/D	N/A[a]	
P08_45	T1	0	15,665	412/28%	452	1,614	169	0.37	7 (3.45×10^{-4})	N/A

N/A, not available; N/D, not detectable. Numbers are given as total, % or normalized to 1×10^6.
[a]Reinitiation of ART.
[b]First ART initiation.

with a continuously declining plasma VL over the period of about 6 months that was accompanied by decreasing proviral DNA loads and IC viral RNA expression (Table 1). In agreement with the clinical treatment files, this individual represented the early virus suppression phase after ART initiation. The GERDA system detected the viral reservoir after 6 months of ART almost exclusively in T_{CM}s. Other memory compartments showed no or only very low signals for Gag+/Env+ translation-competent cells (Figures 4A and 4B), with no signals detectable in co-expanded negative controls (Figure S5B). This was in agreement with LTR-induction events in parallel cultures of QVOA (Figure 3B) with 4.01 infectious units per million in T_{CM}s (confidence interval {1.83, 8.81}),[50] as indicated by viral gene induction and also propagation over time (Figure S5C). Also, higher levels of HIV-1 DNA integration events and IC HIV-1 poly-A transcripts were mainly detected in the T_{CM} subset and less so in other memory compartments (Table 2). Moreover, by tSNE, we confirmed that T_{CM}s further differentiated into transitional memory T cells (T_{TM}s) *in vitro* during viral outgrowth (Figures 4C and 4D) as a logical consequence after stimulation.[51,52]

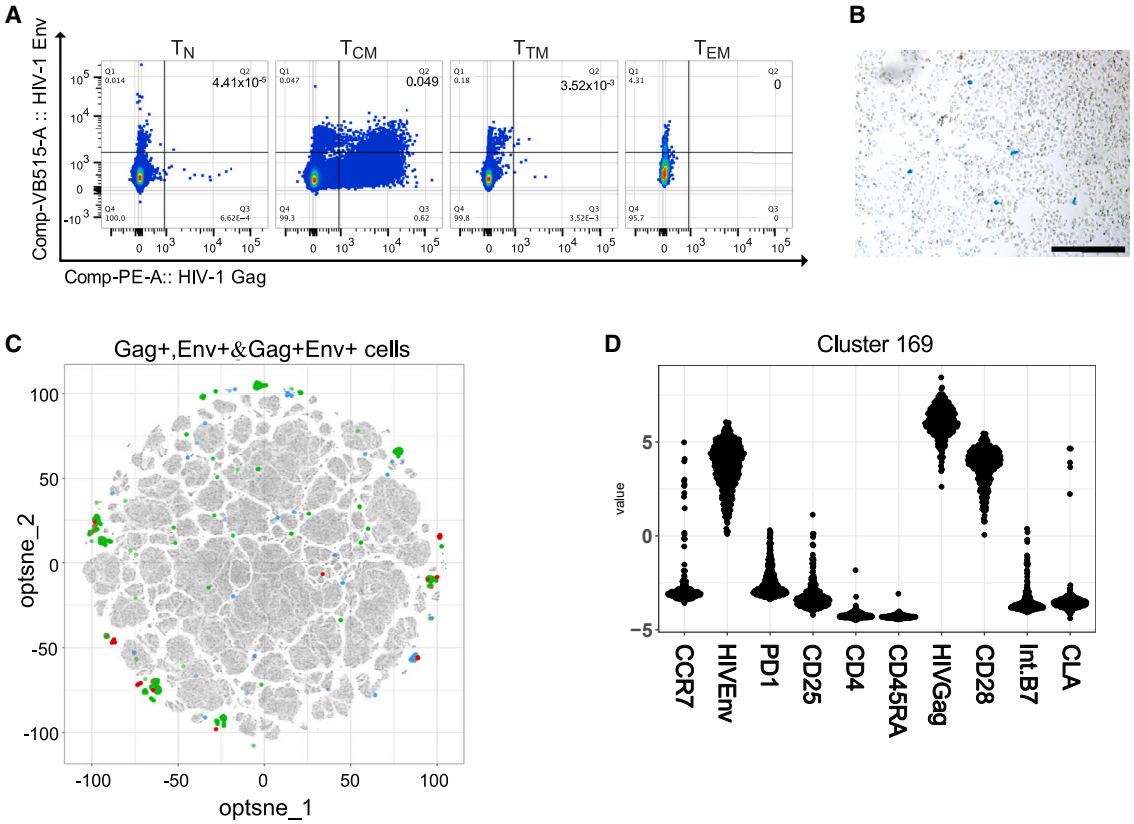

Figure 4. GERDA performance during viral outgrowth for individual P01_46

(A) Gag vs. Env expression events in sorted fractions, 6 months post-ART (from left to right: naive [T_N], central memory [T_{CM}], transitional memory [T_{TM}], and effector memory [T_{EM}]) T cells 14 days post-stimulation.

(B) X-Gal staining of T_{CM} fraction 14 days post-stimulation (extract of Figure S5C); individual infection events in blue. Scale bar represents 250 μm.

(C) tSNE plots of T_{CM} culture on day 14. Dots represent cells as single data points (2.07 × 10^6 cells in total). HIV-1 Gag+ (green), HIV-1 Env+ (blue), and HIV-1 Gag+/Env+ (red) populations are shown.

(D) Marker expression profile of representative cluster.

In conclusion, GERDA was suitable to assign the viral reservoir to T_{CM}s early after infection, which was confirmed 6 months later as the main reservoir by all tested molecular detection formats. This highlights the reliable prediction power of GERDA for viral reservoir deciphering early infection periods.

When expanded T cell fractions, excluding fractions of T_{CM}s, were analyzed for the presence of viral RNA, small amounts of free genomic RNA, indicating the presence of viral particles, were detected exclusively in supernatants of T_Ns (in 3/15 wells) and were accompanied by elevated levels of poly-A transcripts (Table 2). The low HIV-1 RNA levels in the obtained Env sequences corresponded with the low signals for GERDA, poly-A RNA, and LTR induction. This dataset also confirmed the presence of residual replication-competent virus species with identical sequence as already present before therapy initiation (Figure 5A; Table S3).

Individuals P07_07 and P02_53 represent two other highly relevant infection situations: samples of P07_07 had been obtained during the chronic infection phase after extended periods of successful viral suppression, while P02_53 had been identified in a very early phase of an acute virus infection (Fiebig stage II).

PBMC samples from both individuals were sorted and expanded for a QVOA. For P07_07, proviral loads were determined on day 10 of *in vitro* expansion, and only very few proviral integration events were identified in the memory T cell compartments, suggesting a low reactivation potential. This was confirmed since, after cell stimulation, no Gag+/Env+ expression was detected by GERDA, and no cellular LTR induction was observed in the reporter QVOA.

In the clinical primary infection situation of P02_53, the *in vitro* expansion of cells revealed on day 9 some poly-A activity in the T_{CM} compartment, accompanied by a proviral load increase and HIV-1 Gag single-positive signals by GERDA on day 14. However, no virus replication was induced even after three rounds of T cell stimulation and 3 weeks of *in vitro* culture (Table S1). This result is in agreement with clinical observations of low virus expansion immediately after virus transmission and consistent with the relative scarcity of GERDA double-positive events in peripheral blood of successfully treated patients.

Overall, these data show that in individuals infected with HIV-1, at various time points during the disease course, evidence for intact viral genomes and viral activity can be obtained from

Table 2. HIV-1 reservoir in T cell subsets

	Provirus (QVOA day 7)	poly-A (QVOA day 14)		GERDA (QVOA day 14)		QVOA
ID	HIV-1 DNA/10^6	HIV-1 poly-A/10^6	HIV-1 RNA/HIV-1 DNA	HIV-1 Gag+ per 10^6	HIV-1 Gag+/Env+ per 10^6	IUPM
P01_46_T4_TN	250	85,297	341	7	0.4	N/D
P01_46_T4_TCM	155,113	85,513,919	551	6,690	490	4.01
P01_46_T4_TTM	6,433	10,158	2	70	35	N/D
P01_46_T4_TEM	N/D	N/D	N/D	N/D	N/D	N/D

Representative data of individual P01_46. Proviral quantification was done 7 days after stimulation; poly-A and GERDA quantification were done 14 days after stimulation. Results are normalized to 1 × 10^6 cells. IUPM, infectious units per million; ND, not detectable; QVOA, quantitative viral outgrowth assay; poly-A, HIV-1 poly-A transcripts.

peripheral blood samples even after extended periods of full virus suppression, attributable to cells with distinct homing properties that only transiently appear in the circulation. This confirms the existence and critical contribution of non-peripheral virus sanctuary sites with T_{CM}s and T_Ns as key cell pools with mainly lymphoid homing properties (Tables 1 and 2).

This also suggests that viral evolution occurs even during periods of suppressive ART *in vivo*, which could contribute to the continuous change and reshaping pool of reactivatable HIV-1 proviruses.

Virus dynamics inside HIV-1 cell reservoirs

Reactivated infections, as indicated by the LTR-induction in our reporter cells, are based on the functionality of the HIV-1 transactivator Tat. Positive QVOA cultures were further analyzed for the presence of genetically intact viral RNA by single-genome amplification (SGA). For the recent infection situation of P01_46, the same dominating viral variant was identified in all induced culture wells (Figure S5D). Next-generation sequencing (NGS) verified the same dominant virus in clinical samples from peripheral blood during unsuppressed periods at diagnosis (Figure 5A; Table S3). In addition, a unique minority of viral genomes (red box in Figure S6A) appeared in one *in-vitro*-induced well. NGS revealed that this virus variant was already present in the earliest clinical sample (Table S3). The phylogenetic tree of the SGA of outgrowing viruses identified major clusters from three individual cell populations (three wells, Figure 3E) with high sequence conservation in the genomic regions of the rev-response-element (RRE) and Nef (Figures S6B and S6C).

As an example of a spontaneous virus reactivation that could be the cause for the typical rapid virus relapses after therapy interruption, we assessed the IC RNA of individual P04_56 where viral poly-A rose after times of suppression (see Table 1). Due to the low IC HIV-1 poly-A RNA in this individual, only two complete SGA sequence populations could be obtained. The Geno2pheno [co-receptor] algorithm called both HIV populations R5 tropic (false positive rates [FPRs] of 18.9% or 28.5%), and NGS assigned them the highest abundances in the viral populations. Env sequence analysis revealed that both were present at early unsuppressed as well as at late sampling dates (Figure S6D). This indicates that certain intact virus populations stably co-exist over time and can be readily reactivated, e.g., by antigen stimulation. Changes in the relative abundance of virus populations strongly suggest ongoing dynamic events inside the respective viral and proviral reservoirs.

DISCUSSION

This study validates the use of GERDA, a sophisticated flow-based method to evaluate HIV-1-relevant properties of circulating cells that stem from non-peripheral tissues, which may be key indicators and representatives of crucial viral reservoir(s).

The high test sensitivity (one infected cell per million), short hands-on time (compare, e.g., Baxter et al.[24]) and the power of single-cell characterization of GERDA correlate with IC HIV-1 DNA/RNA levels in PBMC populations or with the gold standard QVOA (Figures 1, 2D, 3A, 3B, 3D–3G, 4A, and S5C; Tables 1, 2, and S1). The simultaneous assessment of HIV-1 Gag and Env protein expression pinpoints productively infected T cell classes as dynamic HIV-1 reservoirs and covers the functionality of almost the entire viral genome length, thus avoiding a 5′ or 3′ constrained bias. The combined Gag+/Env+ detection has the additional advantage that both products stem from different viral mRNA species, which Gag alone is not able to represent. Moreover, Env expression alone is more affected by genetic defects than the gag region,[36,53] and assay formats exclusively based on free Gag protein as a reservoir marker only insufficiently assess the presence of infectious particles. Genetic approaches, predicting viral "intactness" based on the absence of gene alterations (indels, inversions, hypermutations, properties of the packaging signal, or major splice donor site defects[37]) miss the fact that, even if long stretches of the Env DNA remain unaltered and appear intact, they may be non-functional due to aberrant or missing protein expression.[54] Conversely, a multitude of studies showed that defective HIV-1 genomes inside cells may still produce individual viral transcripts or proteins,[33–35,55] which could be mistaken as indicators of a functional reservoir of infectious virus.

Benchmarking experiments confirmed a high test specificity and sensitivity of GERDA compared with all other molecular detection methods tested (Figures 2D–2F), even though the number of Gag molecules (about 2,000 per nascent particle[56]) exceeds the smaller number of Env trimers (about 10 per virion).[57] For benchmarking our titration experiments, it is important to note that a single HUT4-3 cell contains multiple HIV-1 transcripts, explaining the high numbers detected even at the

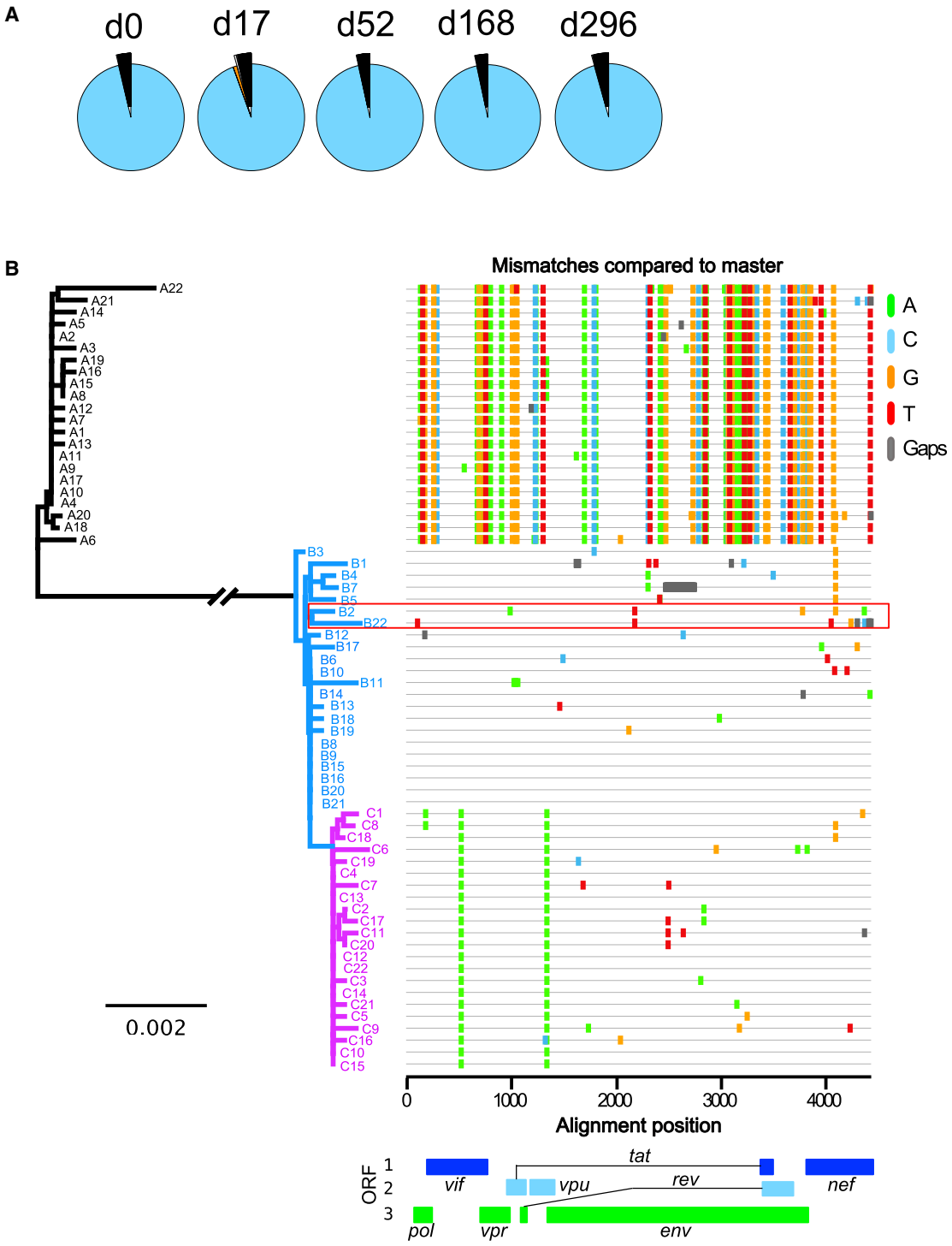

Figure 5. Virus dynamics in HIV-1 cell reservoirs

(A) NGS data of P01_46 over time. Major virus population with relative abundance >1% in same color. Variants below 1% are shown in the inset.

(B) Phylogenetic tree of SGA sequences from individual outgrowth wells (A: black, B: cyan, C: magenta) of P01_46 T_{CM}s in culture supernatant after 14 days of stimulation. Lines represent the 3′ half of the viral genome, and B9 served as reference. Next to the tree, the genome positions of individual SNPs are shown below the plot.

lowest infectious cell numbers. The HIV-1 DNA detection limit of consistently 10 copies in the background of 1×10^6 cellular DNA molecules is fully in the accepted range for diagnostic PCR assays. HIV-1 DNA and HIV-1 poly-A titration curves show a high correlation with $R^2 = 1$ vs. $R^2 = 0.9999$, respectively. This verifies the high reliability of the titration experiments (Figures S2A and S2B). Also, the gold standard QVOA with the LTR-reporter system (via X-Gal), reflecting a reliable functional assay, correlates precisely with a detection limit down to about 3 infectious cells per million cells and proves to be accurate (Figure S3C). The observed strong correlation between Gag+/Env+ double-positive cells on the one hand and molecular infection events of QVOA on the other confirms a high congruence within late protein synthesis events in the GERDA format (Figures 2F and S2A–S2C).

The standardized analysis of the multidimensional data combined tSNE and DBSCAN, allowing us to analyze all data in an identical manner and verify the final data clusters with classical gating. Cluster Beeplots confirmed that each marker had a clear pattern of positive/negative values for each cluster (Figures 3F and 4D), demonstrating good cluster assignment by tSNE and DBSCAN.

Addressing the potential anatomical sanctuary sites, our analysis yielded more lymphoid homing potential of the double-positive cells based on their expression of CCR7 compared with integrin β_7 (gut) or CLA (skin homing) expression.

This observation was particularly striking for recently infected P01_46, who had the highest number of double-positive events for CCR7+ (central) memory cells at the first sampled time point. At 6 months of follow-up, we still detected high signals for provirus, poly-A transcripts, and poly-A per HIV-1 DNA, the highest double-positive cell counts, and numerous viral outgrowth events in the central memory cell fraction in this individual (Figure 4A; Table 2). Stimulation of cells has been reported to potentially downmodulate markers like CCR7. This, however, would also alter the memory fate to T_{TM}s, T_{EM}s, or T_{EMRA}s.[51,52] In our analyses, we mainly found Gag+/Env+ double-positive cells (along with elevated pVL, polyA transcripts, functional SGA/NGS sequences, and outgrowth virus) in T_Ns and T_{CM}s, which are typical, less differentiated cells. The reliability of our cell homing assessment was also reflected in the consistent detection of HIV Gag+/Env+ double-positive cells in T_{CM}s early after diagnosis (with stimulation; Figures 2B, 2F, and 2G) but also 6 months after therapy initiation in sorted and thereby separated cell populations. As the separation by sorting was performed prior to stimulation, the identified populations should reflect the *in vivo* situation (Figures 4A–4C and 5B). Thus, in accordance with our data, the viral reservoirs will still be attributed correctly since CCR7− cells contributed very little on all molecular levels (DNA, RNA, protein, and infectious virus progeny).

This study primarily focused on individuals who had recently started ART therapy. It is known that especially integrin $\alpha_4\beta_7$-expressing cells are predominantly infected and depleted during the early infection phases, with a rather poor recovery during ART.[18,20] Such a situation is exemplified for P02_53, who was sampled during the acute HIV-1 infection phase. This individual had only 1% integrin β_7+ memory cells in the peripheral $CD4^+$ T cells (data not shown). A recent trial with vedoluzimab, a monoclonal antibody directed against integrin $\alpha_4\beta_7$ as potential treatment, controlling viral infection in rhesus macaques,[58] failed to show efficacy of the antibody *in vivo*,[59] thus questioning the role of integrin $\alpha_4\beta_7$ late in chronic stages of HIV-1 disease.

For the acute infection case P02_53, no viral outgrowth was obtained, which could be due to a very early ART initiation, limiting the reservoir establishment. Nevertheless, also in this individual, proviral load and poly-A quantification gave elevated signals for the T_{CM} fraction (Table S1).

Of note, T_{TM} and T_{EM} fractions were number-wise routinely underrepresented in the QVOA samples compared with T_N and T_{CM} fractions.

A key finding of the study presented here is that, although four individuals had detectable VLs in the cell-free plasma (4/7 cases with VLs between 90 and 51,000 copies/mL), no viral gene activity was found inside circulating cells, neither transcriptional (HIV-1 poly-A) nor translational (GERDA), suggesting that a low number of active cells might exist that cannot be sampled, such as, e.g., resident memory T cells.

Interestingly, in late-presenting patients P04_56 and P06_67 (very low CD4 counts), a significant proportion of Gag+ cells were detected with no Env signal, which some assays would have erroneously categorized as "highly active reservoirs" (Figures S4D and S4F).

Of note, HIV-1 poly-A transcripts became detectable in late presenter P04_56 only at time point 5 (Table 1), but information about clinical events that could have triggered this activity spike was not available. One can speculate that immune-stimulatory events might play a role in virus reactivation and could be a source for rapid viral relapses during periods of non-suppressive ART.

A key focus of our study was on the representation of body CD4 T cells harvested from the peripheral blood, attempting to address the CD4 reservoir, to which activated $CD4^+$ cells chiefly contribute.[60,61] The same GERDA format can be applied to tissue-resident macrophages or other cells from certain anatomical niches, which have been proposed to play a critical role in infection.[62] It may also have utility for fresh lymphoid biopsies to study viral activity in organ tissues. Furthermore, the format renders cells suitable for subsequent studies *in situ* inside viable cells, e.g., of viral transcripts by fluorescence *in situ* hybridization (FISH) labeling.[24,38,40]

While most samples in the study were collected during the first month after diagnosis (see Table 1), other parameters such as viral setpoint, CD4 count, recency of infection, or a high immune response, e.g., during primary infection, remained unassigned as additional potentially important contributors.

NGS and SGA data gave us further insights into viral dynamics in reactivated cell populations identified by GERDA or QVOA. As shown in Figure 5B, reactivated viruses can be linked to the respective wells with their genomic footprints, indicating processes such as APOBEC- or RT-induced mutations after reactivation. However, phylogenetic clustering continues to be highly consistent with phylogenetic trees of the viral Rev gene, of Nef, or of the Env V3 region (Figures S6A–S6C). Of note, SGA sequences for V3 data were confirmed by NGS and were stable over time (Figure 5A). GERDA can therefore also be used in combination with omics platforms to assess HIV-1 dynamics on cellular and viral levels.

We conclude that the Gag+/Env+ co-analysis by GERDA deciphers relevant cell populations reflecting active HIV-1 compartments *in vivo* with importance for cure research.

Studies have suggested a close genetic relatedness of recovered viruses, suggesting that viral re- and deactivation and organ homing are interconnected for different body compartments.[13,14,44,45]

Further studies will now focus on the viral dynamics over time by longitudinally studying the clonal evolution of single virus sequences as well as their expression and replication capacity with single-cell resolution.

Limitations of the study

For this study, all our patients recruited for GERDA evaluation were White, male, and of Caucasian ethnicity and contained only subtype B viruses. Only PBMC preparations from peripheral blood, but no biopsy materials, were used in this study. To formally prove assay predictiveness for critical immunologically active organs, a side-by-side comparison with tissue biopsy material will be needed. Most individuals did not present with high viral activity at or shortly after diagnosis and, due to their potent ART viral activity inside cells, had largely declined as shown in Figures 2B and 2C and Table 1.

We therefore anticipate the highest utility for the GERDA method in early diagnostic settings or viral relapse rather than after long periods of viral suppression. Another potential limitation of our study could lie in the inevitable use of mitogens, triggering a general cell stimulation with no specificity for virus or cell type. We attempted to minimize the skew in cell surface marker expression, e.g., of CD25 (cell activation), PD1 (cell exhaustion), or CCR7 (LN homing or marker for specific T cell memory classification) by conducting all cell sorting and selection steps prior to any cell stimulation and by utilizing "untouched selection" protocols that actively retrieve the unwanted cells and leave the desired cell populations behind.

STAR★METHODS

Detailed methods are provided in the online version of this paper and include the following:

- KEY RESOURCES TABLE
- RESOURCE AVAILABILITY
  - Lead contact
  - Materials availability
  - Data and code availability
- METHOD DETAILS
  - Study participants
  - Cells
  - Cell culture
  - PBMC isolation
  - Spinoculation
  - HIV-1 DNA quantification
  - Total/completed HIV-1 RNA transcript quantification
  - Single-genome amplification
  - V3 amplification for next generation sequencing
  - Next-generation sequencing
  - Sequence analysis
  - Viral outgrowth
  - X-gal reporter assay
  - FACS staining
  - Sorting
  - FACS analysis
  - GERDA pipeline and validation
  - Processing of PBMCs for GERDA assay
  - Titration experiments
- QUANTIFICATION AND STATISTICAL ANALYSIS
  - tSNE and DBSCAN
  - Co-receptor usage prediction
  - Statistical analysis

SUPPLEMENTAL INFORMATION

Supplemental information can be found online at https://doi.org/10.1016/j.crmeth.2023.100485.

ACKNOWLEDGMENTS

We thank David Hauser, Enja Kipfer, Lorena Urda, and Christian Mittelholzer (Molecular Virology, DBM University of Basel, Switzerland); Telma Lopes (FACS core facility, DBM, University of Basel, Switzerland); Mario Wickert and Claudia Dumrese (Cytometry Facility, University Hospital Zurich [UZH], Switzerland); Merle Schanz (UZH); Andrin Wacker, Timo Stahl, and Alain Hirschy (Miltenyi); and Rebekka Plattner, Kerstin Asal, and Louise Jayne Seiler (study nurses, University Hospital Basel, Switzerland) for discussion input, technical advice, or the provision of clinical specimens and information. We thank the participants of the SHCS. We thank Gertrud Steger (University of Cologne, Germany) for providing Ramos cells, Alexandra Trkola (University of Zurich, Switzerland) for providing TZM-bl cells through the NIH-HIV reagent program, and Malcolm Martin for providing pBru2, pMal2, and pADic Cl-13 through the NIH-HIV reagent program. We thank Monique Nijhuis (UMC Utrecht, the Netherlands) for providing SupT1 huR5 cells. This work was supported by the Swiss National Science Foundation through SHCS project grant #839 and the China Scholarship Council (CSC201906170031) financially supporting Yuepeng Zhang. This study has been financed within the framework of the Swiss HIV Cohort Study, supported by the Swiss National Science Foundation (grant #201369), by SHCS project #839 and by the SHCS research foundation . The data are gathered by the Five Swiss University Hospitals, two Cantonal Hospitals, 15 affiliated hospitals and 36 private physicians (listed in http://www.shcs.ch/180-health-care-providers).

AUTHOR CONTRIBUTIONS

F.O., Y.Z., and T.K. were responsible for experimental conception and design. F.O. and Y.Z. performed all experiments. F.O., Y.Z., and T.K. analyzed the data and wrote the manuscript. J.S. provided expert assistance with setting up the bioinformatic pipeline for tSNE. A.T. and M.D. processed and analyzed the samples for NGS, applying expertise for data filtering. C.W. helped with FACS panel, staining, and gating optimization. K.K. compiled and provided all patient-related data from the SHCS biobank. M.S. was responsible for recruitment and sample provision of the specimens from all individuals providing blood for the study. F.K. provided bNAbs and shared protocols for bNAb applications. K.J.M. provided total HIV-1 DNA data and contributed to the analysis and interpretation of data. All authors read and contributed to the final form of the manuscript.

DECLARATION OF INTERESTS

K.J.M. has received travel grants and honoraria from Gilead Sciences, Roche Diagnostics, GlaxoSmithKline, Merck Sharp & Dohme, Bristol-Myers Squibb, ViiV, and Abbott, and the University of Zurich received research grants from Gilead Science, Novartis, Roche, and Merck Sharp & Dohme for studies of

K.J.M. T.K. has received honoraria outside of the present study from Gilead Sciences, ViiV Healthcare, and Roche Diagnostics.

Received: June 30, 2022
Revised: January 30, 2023
Accepted: April 28, 2023
Published: May 23, 2023

REFERENCES

1. Perelson, A.S., Neumann, A.U., Markowitz, M., Leonard, J.M., and Ho, D.D. (1996). HIV-1 dynamics in vivo: virion clearance rate, infected cell life-span, and viral generation time. Science *271*, 1582–1586. https://doi.org/10.1126/science.271.5255.1582.
2. Doitsh, G., and Greene, W.C. (2016). Dissecting how CD4 T cells are lost during HIV infection. Cell Host Microbe *19*, 280–291. https://doi.org/10.1016/j.chom.2016.02.012.
3. Maldarelli, F., Wu, X., Su, L., Simonetti, F.R., Shao, W., Hill, S., Spindler, J., Ferris, A.L., Mellors, J.W., Kearney, M.F., et al. (2014). HIV latency. Specific HIV integration sites are linked to clonal expansion and persistence of infected cells. Science *345*, 179–183. https://doi.org/10.1126/science.1254194.
4. Wagner, T.A., McLaughlin, S., Garg, K., Cheung, C.Y.K., Larsen, B.B., Styrchak, S., Huang, H.C., Edlefsen, P.T., Mullins, J.I., and Frenkel, L.M. (2014). Proliferation of cells with HIV integrated into cancer genes contributes to persistent infection. Science *345*, 570–573.
5. Chomont, N., El-Far, M., Ancuta, P., Trautmann, L., Procopio, F.A., Yassine-Diab, B., Boucher, G., Boulassel, M.R., Ghattas, G., Brenchley, J.M., et al. (2009). HIV reservoir size and persistence are driven by T cell survival and homeostatic proliferation. Nat. Med. *15*, 893–900. https://doi.org/10.1038/nm.1972.
6. Bosque, A., Famiglietti, M., Weyrich, A.S., Goulston, C., and Planelles, V. (2011). Homeostatic proliferation fails to efficiently reactivate HIV-1 latently infected central memory CD4+ T cells. PLoS Pathog. *7*, e1002288. https://doi.org/10.1371/journal.ppat.1002288.
7. Vandergeeten, C., Fromentin, R., DaFonseca, S., Lawani, M.B., Sereti, I., Lederman, M.M., Ramgopal, M., Routy, J.P., Sékaly, R.P., and Chomont, N. (2013). Interleukin-7 promotes HIV persistence during antiretroviral therapy. Blood *121*, 4321–4329. https://doi.org/10.1182/blood-2012-11-465625.
8. Wang, Z., Gurule, E.E., Brennan, T.P., Gerold, J.M., Kwon, K.J., Hosmane, N.N., Kumar, M.R., Beg, S.A., Capoferri, A.A., Ray, S.C., et al. (2018). Expanded cellular clones carrying replication-competent HIV-1 persist, wax, and wane. Proc. Natl. Acad. Sci. USA *115*, E2575–E2584. https://doi.org/10.1073/pnas.1720665115.
9. Mendoza, P., Jackson, J.R., Oliveira, T.Y., Gaebler, C., Ramos, V., Caskey, M., Jankovic, M., Nussenzweig, M.C., and Cohn, L.B. (2020). Antigen-responsive cd4+ t cell clones contribute to the hiv-1 latent reservoir. J. Exp. Med. *217*, e20200051. https://doi.org/10.1084/jem.20200051.
10. Finzi, D., Hermankova, M., Pierson, T., Carruth, L.M., Buck, C., Chaisson, R.E., Quinn, T.C., Chadwick, K., Margolick, J., Brookmeyer, R., et al. (1997). Identification of a reservoir for HIV-1 in patients on highly active antiretroviral therapy. Science *278*, 1295–1300. https://doi.org/10.1126/science.278.5341.1295.
11. Wong, J.K., Hezareh, M., Günthard, H.F., Havlir, D.v., Ignacio, C.C., Spina, C.A., and Richman, D.D. (1997). Recovery of replication-competent HIV despite prolonged suppression of plasma viremia. Science *278*, 1291–1295. https://doi.org/10.1126/science.278.5341.1291.
12. Siliciano, J.D., Kajdas, J., Finzi, D., Quinn, T.C., Chadwick, K., Margolick, J.B., Kovacs, C., Gange, S.J., and Siliciano, R.F. (2003). Long-term follow-up studies confirm the stability of the latent reservoir for HIV-1 in resting CD4+ T cells. Nat. Med. *9*, 727–728. https://doi.org/10.1038/nm880.
13. Marie-Angélique De Scheerder, A., Vrancken, B., Dellicour, S., Schlub, T., Lee, E., Shao, W., Rutsaert, S., Verhofstede, C., Kerre, T., Malfait, T., et al. (2019). HIV rebound is predominantly fueled by genetically identical viral expansions from diverse reservoirs. Cell Host Microbe *26*, 347–358.e7. https://doi.org/10.1016/j.chom.2019.08.003.
14. Chaillon, A., Gianella, S., Dellicour, S., Rawlings, S.A., Schlub, T.E., De Oliveira, M.F., Smith, D.M., Ignacio, C., Porrachia, M., and Vrancken, B. (2020). HIV persists throughout deep tissues with repopulation from multiple anatomical sources. J. Clin. Invest. *130*, 1699–1712. https://doi.org/10.1172/JCI134815.
15. Ait-Ammar, A., Kula, A., Darcis, G., Verdikt, R., de Wit, S., Gautier, V., Mallon, P.W.G., Marcello, A., Rohr, O., and van Lint, C. (2019). Current status of latency reversing agents facing the heterogeneity of HIV-1 cellular and tissue reservoirs. Front. Microbiol. *10*, 3060. https://doi.org/10.3389/fmicb.2019.03060.
16. Berg, E.L., McEvoy, L.M., Berlin, C., Bargatze, R.F., and Butcher, E.C. (1993). L-selectin-mediated lymphocyte rolling on MAdCAM-1. Nature *366*, 695–698. https://doi.org/10.1038/366695a0.
17. Berlin, C., Berg, E.L., Briskin, M.J., Andrew, D.P., Kilshaw, P.J., Holzmann, B., Weissman, I.L., Hamann, A., and Butcher, E.C. (1993). $\alpha 4\beta 7$ integrin mediates lymphocyte binding to the mucosal vascular addressin MAdCAM-1. Cell *74*, 185–195. https://doi.org/10.1016/0092-8674(93)90305-A.
18. Guadalupe, M., Reay, E., Sankaran, S., Prindiville, T., Flamm, J., McNeil, A., and Dandekar, S. (2003). Severe CD4+ T-cell depletion in gut lymphoid tissue during primary human immunodeficiency virus type 1 infection and substantial delay in restoration following highly active antiretroviral therapy. J. Virol. *77*, 11708–11717. https://doi.org/10.1128/jvi.77.21.11708-11717.2003.
19. Förster, R., Davalos-Misslitz, A.C., and Rot, A. (2008). CCR7 and its ligands: balancing immunity and tolerance. Nat. Rev. Immunol. *8*, 362–371. https://doi.org/10.1038/nri2297.
20. Sivro, A., Schuetz, A., Sheward, D., Joag, V., Yegorov, S., Liebenberg, L.J., Yende-Zuma, N., Stalker, A., Mwatelah, R.S., Selhorst, P., et al. (2018). Integrin α 4 β 7 expression on peripheral blood CD4 + T cells predicts HIV acquisition and disease progression outcomes. Sci. Transl. Med. *10*, eaam6354.
21. Fuhlbrigge, R.C., Kieffer, J.D., Armerding, D., and Kupper, T.S. (1997). Cutaneous lymphocyte antigen is a specialized form of PSGL-1 expressed on skin-homing T cells. Nature *389*, 978–981. https://doi.org/10.1038/40166.
22. Malnati, M.S., Scarlatti, G., Gatto, F., Salvatori, F., Cassina, G., Rutigliano, T., Volpi, R., and Lusso, P. (2008). A universal real-time PCR assay for the quantification of group-M HIV-1 proviral load. Nat. Protoc. *3*, 1240–1248. https://doi.org/10.1038/nprot.2008.108.
23. Procopio, F.A., Fromentin, R., Kulpa, D.A., Brehm, J.H., Bebin, A.-G., Strain, M.C., Richman, D.D., O'Doherty, U., Palmer, S., Hecht, F.M., et al. (2015). A novel assay to measure the magnitude of the inducible viral reservoir in HIV-infected individuals. EBioMedicine *2*, 874–883. https://doi.org/10.1016/j.ebiom.2015.06.019.
24. Baxter, A.E., Niessl, J., Fromentin, R., Richard, J., Porichis, F., Charlebois, R., Massanella, M., Brassard, N., Alsahafi, N., Delgado, G.-G., et al. (2016). Single-cell characterization of viral translation-competent reservoirs in HIV-infected individuals. Cell Host Microbe *20*, 368–380. https://doi.org/10.1016/j.chom.2016.07.015.
25. Siliciano, J.D., and Siliciano, R.F. (2005). Enhanced culture assay for detection and quantitation of latently infected, resting virus in HIV-1-Infected individuals. Methods Mol. Biol. *304*, 3–15. https://doi.org/10.1385/1-59259-907-9:003.
26. Shan, L., Rabi, S.A., Laird, G.M., Eisele, E.E., Zhang, H., Margolick, J.B., and Siliciano, R.F. (2013). A novel PCR assay for quantification of HIV-1 RNA. J. Virol. *87*, 6521–6525. https://doi.org/10.1128/jvi.00006-13.
27. Descours, B., Petitjean, G., López-Zaragoza, J.L., Bruel, T., Raffel, R., Psomas, C., Reynes, J., Lacabaratz, C., Levy, Y., Schwartz, O., et al. (2017). CD32a is a marker of a CD4 T-cell HIV reservoir harbouring

replication-competent proviruses. Nature *543*, 564–567. https://doi.org/10.1038/nature21710.

28. Bertagnolli, L.N., White, J.A., Simonetti, F.R., Beg, S.A., Lai, J., Tomescu, C., Murray, A.J., Antar, A.A.R., Zhang, H., Margolick, J.B., et al. (2018). The role of CD32 during HIV-1 infection. Nature *561*, E17–E19. https://doi.org/10.1038/s41586-018-0494-3.

29. Abdel-Mohsen, M., Kuri-Cervantes, L., Grau-Exposito, J., Spivak, A.M., Nell, R.A., Tomescu, C., Vadrevu, S.K., Giron, L.B., Serra-Peinado, C., Genescà, M., et al. (2018). CD32 is expressed on cells with transcriptionally active HIV but does not enrich for HIV DNA in resting T cells. Sci. Transl. Med. *10*, eaar6759. https://doi.org/10.1126/scitranslmed.aar6759.

30. Darcis, G., Kootstra, N.A., Hooibrink, B., van Montfort, T., Maurer, I., Groen, K., Jurriaans, S., Bakker, M., van Lint, C., Berkhout, B., and Pasternak, A.O. (2020). CD32 + CD4 + T cells are highly enriched for HIV DNA and can support transcriptional latency. Cell Rep. *30*, 2284–2296.e3. https://doi.org/10.1016/j.celrep.2020.01.071.

31. Bruner, K.M., Murray, A.J., Pollack, R.A., Soliman, M.G., Laskey, S.B., Capoferri, A.A., Lai, J., Strain, M.C., Lada, S.M., Hoh, R., et al. (2016). Defective proviruses rapidly accumulate during acute HIV-1 infection. Nat. Med. *22*, 1043–1049.

32. Ho, Y.-C., Shan, L., Hosmane, N.N., Wang, J., Laskey, S.B., Rosenbloom, D.I.S., Lai, J., Blankson, J.N., Siliciano, J.D., and Siliciano, R.F. (2013). Replication-competent noninduced proviruses in the latent reservoir increase barrier to HIV-1 cure. Cell *155*, 540–551. https://doi.org/10.1016/j.cell.2013.09.020.

33. Pollack, R.A., Jones, R.B., Pertea, M., Bruner, K.M., Martin, A.R., Thomas, A.S., Capoferri, A.A., Beg, S.A., Huang, S.H., Karandish, S., et al. (2017). Defective HIV-1 proviruses are expressed and can Be recognized by cytotoxic T lymphocytes, which shape the proviral landscape. Cell Host Microbe *21*, 494–506.e4. https://doi.org/10.1016/j.chom.2017.03.008.

34. Imamichi, H., Dewar, R.L., Adelsberger, J.W., Rehm, C.A., O'doherty, U., Paxinos, E.E., Fauci, A.S., and Lane, H.C. (2016). Defective HIV-1 proviruses produce novel proteincoding RNA species in HIV-infected patients on combination antiretroviral therapy. Proc. Natl. Acad. Sci. USA *113*, 8783–8788. https://doi.org/10.1073/pnas.1609057113.

35. Imamichi, H., Smith, M., Adelsberger, J.W., Izumi, T., Scrimieri, F., Sherman, B.T., Rehm, C.A., Imamichi, T., Pau, A., Catalfamo, M., et al. (2020). Defective HIV-1 proviruses produce viral proteins. Proc. Natl. Acad. Sci. USA *117*, 3704–3710. https://doi.org/10.1073/pnas.1917876117.

36. Bruner, K.M., Wang, Z., Simonetti, F.R., Bender, A.M., Kwon, K.J., Sengupta, S., Fray, E.J., Beg, S.A., Antar, A.A.R., Jenike, K.M., et al. (2019). A quantitative approach for measuring the reservoir of latent HIV-1 proviruses. Nature *566*, 120–125. https://doi.org/10.1038/s41586-019-0898-8.

37. Hiener, B., Horsburgh, B.A., Eden, J.-S., Barton, K., Schlub, T.E., Lee, E., von Stockenstrom, S., Odevall, L., Milush, J.M., Liegler, T., et al. (2017). Identification of genetically intact HIV-1 proviruses in specific CD4 + T cells from effectively treated participants. Cell Rep. *21*, 813–822. https://doi.org/10.1016/j.celrep.2017.09.081.

38. Grau-Expósito, J., Serra-Peinado, C., Miguel, L., Navarro, J., Curran, A., Burgos, J., Ocaña, I., Ribera, E., Torrella, A., Planas, B., et al. (2017). A novel single-cell FISH-flow assay identifies effector memory CD4+ T cells as a major niche for HIV-1 transcription in HIV-infected patients. mBio *8*, e00876-17. https://doi.org/10.1128/mBio.00876-17.

39. Pardons, M., Baxter, A.E., Massanella, M., Pagliuzza, A., Fromentin, R., Dufour, C., Leyre, L., Routy, J.-P., Kaufmann, D.E., and Chomont, N. (2019). Single-cell characterization and quantification of translation-competent viral reservoirs in treated and untreated HIV infection. PLoS Pathog. *15*, e1007619. https://doi.org/10.1371/journal.ppat.1007619.

40. Liu, R., Yeh, Y.-H.J., Varabyou, A., Collora, J.A., Sherrill-Mix, S., Talbot, C.C., Mehta, S., Albrecht, K., Hao, H., Zhang, H., et al. (2020). Single-cell transcriptional landscapes reveal HIV-1–driven aberrant host gene transcription as a potential therapeutic target. Sci. Transl. Med. *12*, eaaz0802. https://doi.org/10.1126/scitranslmed.aaz0802.

41. Hamy, F., Felder, E.R., Heizmann, G., Lazdins, J., Aboul-ela, F., Varani, G., Karn, J., and Klimkait, T. (1997). An inhibitor of the Tat/TAR RNA interaction that effectively suppresses HIV-1 replication. Proc. Natl. Acad. Sci. USA *94*, 3548–3553. https://doi.org/10.1073/pnas.94.8.3548.

42. Klimkait, T., Stauffer, F., Lupo, E., and Sonderegger-Rubli, C. (1998). Dissecting the mode of action of various HIV-inhibitor classes in a stable cellular system. Arch. Virol. *143*, 2109–2131. https://doi.org/10.1007/s007050050447.

43. Wei, X., Decker, J.M., Liu, H., Zhang, Z., Arani, R.B., Kilby, J.M., Saag, M.S., Wu, X., Shaw, G.M., and Kappes, J.C. (2002). Emergence of resistant human immunodeficiency virus type 1 in patients receiving fusion inhibitor (T-20) monotherapy. Antimicrob. Agents Chemother. *46*, 1896–1905. https://doi.org/10.1128/AAC.46.6.1896-1905.2002.

44. Jones, B.R., Miller, R.L., Kinloch, N.N., Tsai, O., Rigsby, H., Sudderuddin, H., Shahid, A., Ganase, B., Brumme, C.J., Harris, M., et al. (2020). Genetic diversity, compartmentalization, and age of HIV proviruses persisting in CD4 + T cell subsets during long-term combination antiretroviral therapy. J. Virol. *94*, e01786-19–e01805. https://doi.org/10.1128/jvi.01786-19.

45. Abrahams, M.-R., Joseph, S.B., Garrett, N., Tyers, L., Moeser, M., Archin, N., Council, O.D., Matten, D., Zhou, S., Doolabh, D., et al. (2019). The replication-competent HIV-1 latent reservoir is primarily established near the time of therapy initiation. Sci. Transl. Med. *11*, 5589. https://doi.org/10.1126/scitranslmed.aaw5589.

46. van der Maaten, L., and Hinton, G. (2008). Visualizing data using t-SNE. J. Mach. Learn. Res. *9*, 2579–2625.

47. Hahsler, M., Piekenbrock, M., and Doran, D. (2019). Dbscan : Fast density-based clustering with R. J. Stat. Softw. *91*. https://doi.org/10.18637/jss.v091.i01.

48. Bader, J., Däumer, M., Schöni-Affolter, F., Böni, J., Gorgievski-Hrisoho, M., Martinetti, G., Thielen, A., and Klimkait, T.; Swiss HIV Cohort Study (2017). Therapeutic immune recovery and reduction of CXCR4-tropic HIV-1. Clin. Infect. Dis. *64*, 295–300. https://doi.org/10.1093/cid/ciw737.

49. Bachmann, N., von Siebenthal, C., Vongrad, V., Turk, T., Neumann, K., Beerenwinkel, N., Bogojeska, J., Fellay, J., Roth, V., Kok, Y.L., et al. (2019). Determinants of HIV-1 reservoir size and long-term dynamics during suppressive ART. Nat. Commun. *10*, 3193. https://doi.org/10.1038/s41467-019-10884-9.

50. Rosenbloom, D.I.S., Elliott, O., Hill, A.L., Henrich, T.J., Siliciano, J.M., and Siliciano, R.F. (2015). Designing and interpreting limiting dilution assays: general principles and applications to the latent reservoir for HIV-1. Preprint at bioRxiv. https://doi.org/10.1101/018911.

51. Mahnke, Y.D., Brodie, T.M., Sallusto, F., Roederer, M., and Lugli, E. (2013). The who's who of T-cell differentiation: human memory T-cell subsets. Eur. J. Immunol. *43*, 2797–2809. https://doi.org/10.1002/eji.201343751.

52. Jameson, S.C., and Masopust, D. (2018). Understanding subset diversity in T cell memory. Immunity *48*, 214–226. https://doi.org/10.1016/j.immuni.2018.02.010.

53. Lu, C.L., Pai, J.A., Nogueira, L., Mendoza, P., Gruell, H., Oliveira, T.Y., Barton, J., Lorenzi, J.C.C., Cohen, Y.Z., Cohn, L.B., et al. (2018). Relationship between intact HIV-1 proviruses in circulating CD4+ T cells and rebound viruses emerging during treatment interruption. Proc. Natl. Acad. Sci. USA *115*, E11341–E11348. https://doi.org/10.1073/pnas.1813512115.

54. de Verneuil, A., Migraine, J., Mammano, F., Molina, J.-M., Gallien, S., Mouquet, H., Hance, A.J., Clavel, F., and Dutrieux, J. (2018). Genetically intact but functionally impaired HIV-1 env glycoproteins in the T-cell reservoir. J. Virol. *92*, e01684-17. https://doi.org/10.1128/JVI.01684-17.

55. Wiegand, A., Spindler, J., Hong, F.F., Shao, W., Cyktor, J.C., Cillo, A.R., Halvas, E.K., Coffin, J.M., Mellors, J.W., and Kearney, M.F. (2017). Single-cell analysis of HIV-1 transcriptional activity reveals expression of proviruses in expanded clones during ART. Proc. Natl. Acad. Sci. USA *114*, E3659–E3668. https://doi.org/10.1073/pnas.1617961114.

56. Sun, W., Reyes-Serratos, E., Barilla, D., Santos, J.R.L., Bujold, M., Graves, S., and Marcet-Palacios, M. (2019). Mathematical determination of the

HIV-1 matrix shell structure and its impact on the biology of HIV-1. PLoS One *14*, e0224965. https://doi.org/10.1371/journal.pone.0224965.

57. Zhu, P., Chertova, E., Bess, J., Lifson, J.D., Arthur, L.O., Liu, J., Taylor, K.A., and Roux, K.H. (2003). Electron tomography analysis of envelope glycoprotein trimers on HIV and simian immunodeficiency virus virions. Proc. Natl. Acad. Sci. USA *100*, 15812–15817. https://doi.org/10.1073/pnas.2634931100.
58. Byrareddy, S.N., Arthos, J., Cicala, C., Villinger, F., Ortiz, K.T., Little, D., Sidell, N., Kane, M.A., Yu, J., Jones, J.W., et al. (2016). Sustained virologic control in SIV+ macaques after antiretroviral and α4β7 antibody therapy. Science *354*, 197–202. https://doi.org/10.1126/science.aag1276.
59. Sneller, M.C., Clarridge, K.E., Seamon, C., Shi, V., Zorawski, M.D., Justement, J.S., Blazkova, J., Huiting, E.D., Proschan, M.A., Mora, J.R., et al. (2019). An open-label phase 1 clinical trial of the anti-α4β7 monoclonal antibody vedolizumab in HIV-infected individuals. Sci. Transl. Med. *11*, 3447. https://doi.org/10.1126/scitranslmed.aax3447.
60. Lee, E., Bacchetti, P., Milush, J., Shao, W., Boritz, E., Douek, D., Fromentin, R., Liegler, T., Hoh, R., Deeks, S.G., et al. (2019). Memory CD4 + T-cells expressing HLA-DR contribute to HIV persistence during prolonged antiretroviral therapy. Front. Microbiol. *10*, 2214. https://doi.org/10.3389/fmicb.2019.02214.
61. Horsburgh, B.A., Lee, E., Hiener, B., Eden, J.-S., Schlub, T.E., von Stockenstrom, S., Odevall, L., Milush, J.M., Liegler, T., Sinclair, E., et al. (2020). High levels of genetically intact HIV in HLA-DR+ memory T cells indicates their value for reservoir studies. AIDS *34*, 659–668. https://doi.org/10.1097/QAD.0000000000002465.
62. Ganor, Y., Real, F., Sennepin, A., Dutertre, C.A., Prevedel, L., Xu, L., Tudor, D., Charmeteau, B., Couedel-Courteille, A., Marion, S., et al. (2019). HIV-1 reservoirs in urethral macrophages of patients under suppressive antiretroviral therapy. Nat. Microbiol. *4*, 633–644. https://doi.org/10.1038/s41564-018-0335-z.
63. Wickham, H. (2009). ggplot2. https://doi.org/10.1007/978-0-387-98141-3.
64. Liszewski, M.K., Yu, J.J., and O'Doherty, U. (2009). Detecting HIV-1 integration by repetitive-sampling Alu-gag PCR. Methods *47*, 254–260. https://doi.org/10.1016/J.YMETH.2009.01.002.
65. Song, H., Giorgi, E.E., Ganusov, V.v., Cai, F., Athreya, G., Yoon, H., Carja, O., Hora, B., Hraber, P., Romero-Severson, E., et al. (2018). Tracking HIV-1 recombination to resolve its contribution to HIV-1 evolution in natural infection. Nat. Commun. *9*, 1928. https://doi.org/10.1038/s41467-018-04217-5.
66. Belkina, A.C., Ciccolella, C.O., Anno, R., Halpert, R., Spidlen, J., and Snyder-Cappione, J.E. (2019). Automated optimized parameters for T-distributed stochastic neighbor embedding improve visualization and analysis of large datasets. Nat. Commun. *10*, 5415. https://doi.org/10.1038/s41467-019-13055-y.

STAR★METHODS

KEY RESOURCES TABLE

REAGENT or RESOURCE	SOURCE	IDENTIFIER
Antibodies		
CD3 (BV510)(UCHT-1)	Biolegend	Cat#: 300447, RRID: AB_2563467
CD4 (BV650)(RPA-T4)	Biolegend	Cat#: 300535, RRID: AB_2561351
CD8 (A700)(RPA-T8)	Biolegend	Cat#: 301027, RRID: AB_493744
CD14 (APC-Cy7)(M5E2)	Biolegend	Cat#: 301819, RRID: AB_493694
CD19 (APC-Cy7)(HIB19)	Biolegend	Cat#: 302217, RRID: AB_314247
CD25 (BV605)(BC96)	Biolegend	Cat#: 302631, RRID: AB_11123913
CD28 (PE-Dazzle)(CD28.2)	Biolegend	Cat#: 302941, RRID: AB_2564234
CD45RA (BV711)(HI100)	Biolegend	Cat#: 304137, RRID: AB_11218999
CCR6 (PerCP-Cy5.5)(G034E3)	Biolegend	Cat#: 353405, RRID: AB_10918985
CCR7 (APC)(G043H7)	Biolegend	Cat#: 353213, RRID: AB_10915474
CLA (PerCP-Cy5.5)(HECA-452)	Biolegend	Cat#: 321313, RRID: AB_2565765
Integrin β7 (PE-Cy7)(FIB504)	ThermoFisher	Cat#: 25-5867-42, RRID: AB_2573481
PD1 (BV421)(EH12.2H7)	Biolegend	Cat#: 329919, RRID: AB_10900818
HIV Gag (PE)(KC57)	Beckman Coulter	Cat#: 6604667, RRID: AB_1575989
CD45 (PerCP-Cy5.5)(HI30)	Biolegend	Cat#: 304027, RRID: AB_1236444
CD45 (A700)(HI30)	Biolegend	Cat#: 304023, RRID: AB_493760
CD45 (BV421)(HI30)	Biolegend	Cat#: 304031, RRID: AB_10900423
CD45 (BV605)(HI30)	Biolegend	Cat#: 304041, RRID: AB_2562105
CD45 (BV785)(HI30)	Biolegend	Cat#: 304047, RRID: AB_2563128
CD45 (BUV395)(HI30)	BD	Cat#: 563792, RRID: AB_2869519
Zombie NIR	Biolegend	Cat#: 423105
Biotin antibody (VioBright515)(REA746)	Miltenyi Biotec	Cat#: 130-111-074, RRID: AB_2661395
3BNC117 (CD4bs)	Prof. Florian Klein	N/A
10-1074 (V3-loop)	Prof. Florian Klein	N/A
PG16 (V1V2-loop)	Prof. Florian Klein	N/A
35O22 (gp120-gp41 interface)	Prof. Florian Klein	N/A
10E8 (MPER gp41)	Prof. Florian Klein	N/A
MGO (human IgG1 Iso-type control)	Prof. Florian Klein	N/A
Mouse IgG1 k-PE (Iso ctrl HIV Gag)	Biolegend	Cat#: 400111, RRID: AB_2847829
Bacterial and virus strains		
Plasmid derived NL-NF (pNL4-3 derivative)	Porf. Thomas Klimkait	N/A
Plasmid derived LAI	Porf. Thomas Klimkait	N/A
Plasmid derived Mal2	Porf. Thomas Klimkait	N/A
Plasmid derived ADIc Cl-13 (Ala-1)	Porf. Thomas Klimkait	N/A
Biological samples		
Full blood or cryopreserved PBMCs of HIV-1 infected individuals	SHCS contributing centers	N/A
Chemicals, peptides, and recombinant proteins		
PHA (phytohaemagglutinin)	Sigma	Cat#: 478149-53-0
Pen/Strep	Bioconcept	Cat#: 4-01F00H
Maraviroc (MVC)	Selleckchem	Cat#: S2003
Efavirenz (EFV)	Selleckchem	Cat#: S4685
Plerixafor (AMD3100)	Selleckchem	Cat#: S8030

(*Continued on next page*)

Continued

REAGENT or RESOURCE	SOURCE	IDENTIFIER
Z-VAD-FMK	Selleckchem	Cat#: S7023
5-Brom-4-chlor-3-indolyl-β-D-galactopyranosid (X-gal)	Sigma	Cat#: B4252-1G
Human IL-2 IS, premium grade	Miltenyi Biotec	Cat#: 130-097-743
Critical commercial assays		
Maxwell® RSC Cultured Cells DNA Kit	Promega	Cat#: AS1620
GoTaq® Probe qPCR Master Mix	Promega	Cat#: A6102
Maxwell® RSC simply RNA cells kit	Promega	Cat#: AS1390
qRT-PCR Brilliant III probe master mix kit	Agilent	Cat#: 600884
ImmunoCult™-XF T cell Expansion Medium	STEMCELL Technologies	Cat#: 10981
ImmunoCult™ Human CD3/CD28/CD2 T cell Activator	STEMCELL Technologies	Cat#: 10970
MACSxpress® Whole Blood CD4 T cell Isolation Kit, human	Miltenyi Biotec	Cat#: 130-098-195
Zero Blunt™ TOPO™ PCR Cloning Kit	Thermo Fisher	Cat#: 450245
$CD4^+$ T cell Isolation Kit, human	Miltenyi Biotec	Cat#: 130-096-533
EZ-Link® Micro Sulfo-NHS-LC-Biotinylation Kit	Thermo Fisher	Cat#: 21935
Zeba™ Spin Desalting Columns, 7K MWCO, 2 mL	Thermo Fisher	Cat #: 89890
jetPRIME® Transfection reagent	Polyplus	Cat#: 101000001
Experimental models: Cell lines		
HUT4-3	Prof. Thomas Klimkait	Hamy et al., 1997[41]
SupT1 hu R5	Prof. Monique Nijhuis	N/A
TZM-bl	NIH	ARP-8129
Ramos	Dr. Gertrud Steger	N/A
SXR5 (SX22-1)	Prof. Thomas Klimkait	Klimkait et al., 1998[42]
HUT4-3	Prof. Thomas Klimkait	Hamy et al., 1997[41]
Oligonucleotides		
See Table S4 for all oligonucleotides used in study		N/A
Recombinant DNA		
pMVQA	This paper	Addgene ID 197894
pNL-NF (pNL4-3 derivative)	Prof. Thomas Klimkait	N/A
pLAI	Prof. Malcolm Martin	N/A
pMal2	Prof. Malcolm Martin	N/A
pADIc Cl-13 (Ala-1)	Prof. Malcolm Martin	N/A
Software and algorithms		
Rstudio (2022.12.0 + 353)	Posit Software, PBC	https://www.rstudio.com
GraphPad Prism v8	Graphpad Software La Jolla, California, USA	https://www.graphpad.com
Affinity Designer 2	Pantone LLC	https://affinity.serif.com
FlowJo 10.8.2	FlowJo Software, Becton Dickinson & Company (BD)	https://www.flowjo.com
FACSDiva Software v8.0.1	FACSDiva Software, Becton Dickinson & Company (BD)	https://www.bdbiosciences.com
Optsne	Dotmatics	www.omiq.ai
DBscan	Hahsler et al., 2019[47]	
Dbscan.opt	https://github.com/JulianSpagnuolo/FACkit	N/A
R package ggplot	Wickham, 2009[63]	N/A

(*Continued on next page*)

Continued

REAGENT or RESOURCE	SOURCE	IDENTIFIER
R package ggpubr	https://github.com/eclarke/ggbeeswarm	N/A
R package pheatmaps	https://github.com/raivokolde/pheatmap	N/A
Deposited Data		
GERDA datasets	This paper	https://doi.org/10.17632/8c4zbxfvwk.3
NGS data	This paper	A full list of GenBank accession numbers is available at https://doi.org/10.17632/8c4zbxfvwk.3
SGA data	This paper	A full list of GenBank accession numbers is available at https://doi.org/10.17632/8c4zbxfvwk.3
Other		
NGS sequencing service	Seq-IT GmbH & Co.KG	N/A
DMEM, high glucose	Bioconcept	Cat#: 1-26F50-I
PBS	Bioconcept	Cat#: 3-05F29-I
RPMI-1640,	Bioconcept	Cat#: BC-1-41F51-I
T4 DNA ligase	NEB	Cat#: M0202T
Taq DNA Polymerase with ThermoPol®Buffer	NEB	Cat#: M0267S
FBS	Gibco	Cat#: 26140079
UltraComp eBeads™ Compensation Beads	Thermo Fisher	Cat#: 01-2222-42
Histopaque® 1.077 g/mol	Sigma	Cat#: 10771
FcR Blocking reagent	Miltenyi Biotec	Cat#: 130-059-901

RESOURCE AVAILABILITY

Lead contact

Further information and requests for resources and reagents should be directed to and will be fulfilled by the lead contact, Thomas Klimkait (thomas.klimkait@unibas.ch).

Materials availability

Plasmids used in this study have been deposited in Addgene. Catalog numbers are listed in the key resources table.

Data and code availability

- All GERDA datasets have been deposited at Mendeley Data and are publicly available as of the date of publication, see key resources table for DOIs. NGS sequencing data and SGA sequencing data have also been deposited at GenBank and a full list of accession numbers is available via the Mendeley deposition (see again DOIs listed in the key resources table).
- Custom analysis code for this paper is deposited at Mendeley Data and the DOIs are listed in the key resources table.
- Any additional information required to reanalyze the data reported in this paper is available from the lead contact upon request.

METHOD DETAILS

Study participants

SHCS project no 839 approval was obtained from the local ethics committees of all study sites of the Swiss HIV Cohort Study (Kantonale Ethikkommission Bern, Ethikkommission beider Basel, Ethikkommission des Kantons St. Gallen, Kantonale Ethikkommission Zurich, Comitato etico cantonale del Ticino, Commission d'ethique de la recherche clinique de la faculte de biologie et de medicine de l'universite de Lausanne and Comite d'ethique du department de medicine des hopitaux universitaires de Geneve), and written consent from all participating patients is available.For the study samples from 2 female and 10 male cohort individuals were included. The median age at infection was 45 ± 11.7 years, with a median baseline viral load of 24,200 copies/mL. For further details please see Table S2.

Cells

HUT4-3 cells are HUT78 (M. Martin, NIAID, Bethesda, MD, USA) derivatives, constitutively expressing infectious HIV-1. In brief, they were derived after infection with the clonal HIV-1 isolate NL4-3 (M. Martin); after *in vitro* infection surviving cells were repeatedly passaged until stable, CD4-negative cells emerged. Cells were cloned by limiting dilution and characterized for high virus production (laboratory of T. Klimkait, University of Basel, Switzerland). SupT1 hu R5 cells were from Monique Nijhuis, UMC Utrecht, NL. TZM-bl cells were obtained through the NIBSC center for AIDS reagents,[43] Ramos cells were obtained from Gertrud Steger (University of Cologne, GER).

Cell culture

HUT4-3 cells, Ramos cells and SupT1 cells were maintained in RPMI 1640 medium supplement with 10% FBS, penicillin (100 U/mL) and streptomycin (100 U/mL) (Bioconept, Allschwil, CH). TZM-bl and SXR-5 cells were maintained in DMEM medium supplement with 10% FBS, penicillin (100U/mL), and streptomycin (100U/mL). Cultures were maintained in 5% CO_2 at 37°C.

PBMC isolation

Up to 40 mL of fresh blood was drawn from consenting, recently diagnosed HIV-1 positive individuals. PBMC were isolated by density gradient centrifugation using Histopaque 1.077 g/mol (Sigma) on the day of harvest or on day 1 and were either stained directly or, for storage, frozen in FBS with 10% DMSO.

Spinoculation

SupT1 (unstimulated) or HIV negative PBMC (2 days PHA pre-stimulated) were used for spinoculation: Viral stocks (NL4-3 X4-tropic, LAI X4-tropic, Ala-1 X4-tropic, Mal-2 R5-tropic) were spun onto target cells for 90 min at 800xg in minimal volume of culture media in a 24-well plate. Fresh RPMI 1640 supplemented with 10% FBS and Pen/Strep was then added to each well and cells were kept for 2 days at 37°C, 5% CO_2. Cells were washed extensively with PBS and cultured in fresh medium for an additional 3 days. Cells were now used for FACS and GERDA analysis. Viral infectivity in the supernatant was evaluated by using the SXR5 cell line containing an LTR-lacZ reporter (see below).

HIV-1 DNA quantification

The proviral load was measured as described by others.[22] In brief, primer and probe pairs targeting either HIV-1 LTR[64] or CCR5 were used in a single-plex real-time PCR approach. HUT4-3 gDNA was used as standard (2 HIV-1 copies per cell). HIV-1 DNA were extracted by Maxwell RSC Cultured Cells DNA Kit (Promega, Madison, USA). The GoTaq Probe qPCR Master Mix (Promega, Madison, USA) was used for quantification, cycling conditions were as follows: 1 min at 95°C, 45 cycles of alternating 15 s at 95°C and 1 min at 60°C. We performed the assay and analyzed the data with 7500 Fast Real-time PCR System (Themo Fisher, Walthan, MA, USA).

Total/completed HIV-1 RNA transcript quantification

Intracellular poly-A HIV-1 transcripts were measured according to a published method.[26] Briefly, intracellular total nucleic acids from frozen PBMC were isolated with Promega Maxwell RSC simply RNA cells kit (Promega, Madison, USA), and aliquots immediately frozen at −20°C or −80°C. HIV-1 poly-A transcripts were quantified by One-step RT qPCR using standards of inhouse plasmid pMVQA; reads were normalized to cell count using CCR5 as described elsewhere.[22] The qRT-PCR Brilliant III probe master mix kit (Agilent, Santa Clara, USA) was used for the quantification of HIV-1 RNA transcripts, qPCR was performed using the 7500 Fast Real-time PCR System (Themo Fisher, Walthan, MA, USA) with the following cycling conditions: 50°C for 10 min, 95°C for 3 min, 45 cycles of 95°C 15 s, 60°C 30 s.

Single-genome amplification

Viral RNA was extracted from culture supernatant using Maxwell RSC miRNA Plasma and Serum Kit (Promega, Madison, WI, USA), which included a DNaseI digestion step to have only RNA present. SGA of 3′ half genome sequences was performed as previously described.[65] Complementary DNA was synthesized using the SuperScript IV First-strand Synthesis System (Invitrogen, Carlsbad, CA) with primer R-9632 5′-ACTACTTGAAGCACTCAAGGCAAGCTTTATTG-3′. cDNA was serially diluted with the goal of less than 30% positive amplification by nested PCR using Herculase II Fusion DNA Polymerase (Agilent, California, USA). At this dilution, most positive wells contain amplicons derived from a single cDNA molecule. First round PCR included sense primer F-4875 5′-CAAATTAYAAAAATTCAAAATTTTCGGGTTTATTACAG-3′ and antisense primer R-9626 5′- TGAAGCACTCAAGGCAAGCT TTATTGAGGC-3′. Following PCR conditions were used: 94°C for 2 min followed by 35 cycles of 94°C 15 s, 58°C 30 s, 68°C 4 min, with a final extension of 68°C for 10 min. The second PCR included sense primer F-4900 5′-GGGTTTATTACAGGGACAGCA GAG-3′ and antisense primer R-9602 5′-TGAGGCTTAAGCAGTGGGTTCC-3′. PCR conditions were used: 94°C for 2min followed by 45 cycles of 94°C 15 s, 58°C 30 s, 68°C 4 min, with a final extension of 68°C for 10 min. All PCR products are verified on a 1% agarose gel and sent directly for sequencing.

V3 amplification for next generation sequencing

For amplification a nested PCR approach was chosen. The Herculase II Fusion DNA Polymerase Kit (Agilent Technologies) was used in a 25 μL reaction volume. 24 μL of Master Mix were mixed with 1 μL of extracted patient gDNA or purified first PCR. Each PCR was

carried out in triplicates to normalize for PCR amplification bias. First PCR included sense primer F-6553 5′- ATGGG ATCAAAGCCTAAAGCCATGTG-3′ and R-7801 5′- AGTGCTTCCTGCTGCTCCCAAGAACCCAAG-3′. Following cycling conditions were used: initial 3 min at 95°C, 30 cycles of denaturation for 15 s at 95°C, annealing for 20 s at 60°C and extension for 45 s at 72°C. Final extension was done for 3 min at 72°C.

The second PCR included sense primer F-6848 (5′- AGGCCTGTCCAAAGGTATCCTTTGA-3′; second PCR) and antisense primer R- 7371 (5′- TTACAGTAGAAAAATTCCCCTCCACAATTAAA-3′; second PCR). Cycling conditions for the second PCR were the same as for the first PCR except an annealing temperature of 56°C for 20 s.

Next-generation sequencing

For DNA quantification of NGS samples the Quant-iT PicoGreen dsDNA Assay Kit (Invitrogen) was used according to protocol. DNA concentration was adjusted to 0.2 ng/μL and the Nextera XT DNA Library Preparation Kit (Illumina) was used to prepare the library according manufacturer's protocol. Sequencing was performed with an Illumina MiSeq Benchtop sequencer with 2 × 250bp reads.

Sequence analysis

PCR amplicons were sequenced by the Sanger sequencing on an ABI 3730xl sequencer or by NGS with an Illumina MiSeq Benchtop sequencer. The full-length envelope sequences were assembled and aligned using Genious Prime2021.0.3 version. Phylogenetic trees were based on nucleotide sequences and constructed using the neighbor-joining method. Highlighter plots were compiled at https://www.hiv.lanl.gov/content/sequence/HIGHLIGHT/highlighter_top.html.

Viral outgrowth

Sorted cell fractions were plated in 96-well format. Per well 1–3X10E5 patient's cells were plated with addition of 10E4 SupT1 hu R5 in 50% ImmunoCult-XF T cell Expansion Medium, 50% conditioned medium, 100IU IL-2/mL and anti-human CD3/CD28/CD2 Antibody stimulation cocktail (Stem Cell Technologies). After 3 days fresh medium with 50 IU IL-2 was added and every 2–3 days medium was exchanged. On days 7 and 14 cells were re-stimulated. From the seventh day onward, viral outgrowth was measured by X-Gal stain to follow viral propagation over time.

X-gal reporter assay

The reporter assay for HIV-induction is based on the induction of an integrated LTR-lacZ gene in the stable reporter line SXR5, which is driven by an HIV-1 infection *in vitro*. The assay was performed as described.[42] SXR5 (or TZM-bl) cells were used to detect HIV-1 infection events after *in vitro* infection by the induction of HIV-1 LTR dependent β-Galactosidase activity. 2–3X10E6 SXR5 or TZM-bl cells were plated in a 24- or 48-well plate the day before co-culture. Cells were co-cultured for 2 days after addition of putatively infected cells; alternatively, viral supernatants were spinoculated as described above. At harvest, cells were fixed with 2% formaldehyde and X-Gal was added for readout. X-Gal stains were imaged on a CTL Immunospot S6 Ultimate UV Image analyzer (CTL). A true infection event was considered when blue colored cell event consisted of more than 1 cell or if clear syncytia had formed (viral X4 tropism).

FACS staining

For titration, infectious HUT4-3 cells were pre-stained with CellTrace Far Red Cell Proliferation Kit (Invitrogen) at 37°C. Then, HUT4-3 cells were spiked into Ramos (B-)cells and stained for live/dead cell exclusion (Viobility 405/452, Miltenyi). FcR was blocked for 5–10 min at RT and respective cell surface markers were stained as described below. For all experiments with PBMCs obtained from HIV+ individuals, cells were kept at 37°C during all PBS washing steps. FcR was blocked for 5–10 min at RT, followed by 15 min Live/Dead (Zombie NIR, Biolegend) and CCR7 staining. Subsequently, all other surface markers were incubated for additional 20 min at RT. Cells were washed in all subsequent steps in staining buffer (PBS, 2 mM EDTA, 1% human serum). For FACS analysis, the following antibody panel was used: CD3 (BV510, Biolegend) CD4 (BV650, Biolegend), CD8 (A700, Biolegend), CD14/CD19 (APC-Cy7, Biolegend), CD25 (BV605, Biolegend), CD28 (PE-Dazzle, Biolegend), CD45RA (BV711, Biolegend), CCR6(PerCP-Cy5.5, Biolegend), CCR7 (APC, Biolegend), CLA (PerCP-Cy5.5, Biolegend), Integrin β7 (PE-Cy7, Biolegend), PD1 (BV421, Biolegend), HIV-1 Gag (PE, Beckman Coulter). An LSR Fortessa (BD Bioscience) was used for cell analysis. For sorts, a FITC-labeled alternative antibody against CD4 (Biolegend) was used.

Sorting

Up to 40 mL of whole blood was drawn from HIV-1 positive individuals on cART, and CD4 cells were isolated by whole blood untouched selection (Miltenyi). Preselected cells were cultured overnight in ImmunoCult-XF T cell Expansion Medium (Stem Cell Technologies), 1 μM AMD, 1 μM MVC, 0.5 μM EFV and 50 IU IL-2/mL (Miltenyi) at 37°C 5% CO2. The next day cells were harvested, washed and stained. Cells were strictly kept on ice until sorting. Cells were sorted on a FACS AriaIII (BD Bioscience) cell sorter under BSL-3 conditions.

FACS analysis

Flow cytometry data were analyzed using FlowJo v10.6.1 software (TreeStar). Cell populations of interest (viable $CD3^{+}CD4+/-CD8^{-}CD14^{-}CD19^{-}$) were exported in CSV format for tSNE downstream applications.

GERDA pipeline and validation

Biotinylation of bNAbs

All bNAbs (3BNC117 (CD4bs), 10–1074 (V3-loop), PG16 (V1V2-loop), 35O22 (gp120-gp41 interface), 10E8 (MPER gp41) were biotinylated with EZ-Link Micro Sulfo-NHS-LC-Biotinylation Kit (Thermo Fisher). Briefly, a total of 2.5 μg bNAb mix of equal quantities was biotinylated with a 30-fold molar excess of Sulfo-NHS-LC-Biotin in 500 μL volume for 60 min at room temperature (RT). To remove excess Biotin, biotinylated bNAbs were purified over a Zeba Spin Desalting Column. Biotinylated bNAbs were stored at 4°C until further use.

Processing of PBMCs for GERDA assay

A CD4-untouched pre-selection step was performed to enrich for $CD4^+$ cells. Selected cells were then stimulated in 50% ImmunoCult-XF T cell Expansion Medium (Stem Cell Technologies), 50% conditioned medium, 2.5 μg/mL PHA (Sigma), 5 μM AMD3100 (Selleckchem), 5 μM MVC (Selleckchem), 1 μM EFV (Selleckchem), 5 μM Z-VAD-FMK (Selleckchem), 100 IU IL-2/mL (Miltenyi) for 36-40h to reactivate latent proviruses. HUT4-3 cells, as positive control, were stimulated with PHA 24h prior to staining. For optimized conditions ≥2.5X10E6 Ramos cells ($CD19^+CD3^-$) were added as carrier cells. Subsequently, cells were surface stained for immunological characterization or for assessing Env expression. To detect Env, we used 5 μg/mL biotinylated bNAb mix (3BNC117, 10–1074, PG16, 35O22, 10E8 all provided by F. Klein) which was targeted by an Anti-Biotin-VioBright 515 (Miltenyi) secondary antibody. Cells were fixed for 30 min at RT in PBS 2% PFA. Cells were permeabilized twice with ICS Permeabilization Wash buffer (Biolegend) labeled intracellularly with anti-HIV Gag (KC-57PE, Beckman Coulter). ICS labeled samples were washed twice in perm-wash buffer and acquired on an LSRFortessa (BD Bioscience).

Titration experiments

For titration, the infectious cell clone HUT4-3[41] was spiked into the HIV-1 non-susceptible B-cell line (Ramos) to estimate infectious cells per million (quantities of either 100,000, 2,250, 225, 45, 9, 3, 1, 0.3 presumed infectious HUT4-3 cells). Each dilution was examined by qPCR for HIV-1 DNA load, RT-qPCR for poly-A transcripts, GERDA for Gag+/Env+ translation-competent cells and HIV-1 LTR driven X-Gal readout for HIV-1 infection events.

QUANTIFICATION AND STATISTICAL ANALYSIS

tSNE and DBSCAN

FACS data was imported into RStudio (2022.12.0 + 353, Posit Software, PBC) and first arcsin transformed (custom code Julian Spagnuolo, https://doi.org/10.17632/8c4zbxfvwk.1). For data dimension reduction thresholds for each channel were set and normalized data was dimensionally reduced by opt-SNE[66] using OMIQ.ai (Dotmatics). tSNE plots were produced with the ggplot2 package.[63] For refined clustering of the dimensional reduced data a density based semi-supervised clustering algorithm DBSCAN[47] was used. Parameters Minimal points and Epsilon for DBSCAN usage were determined by running knndistplot and looking for "first" valley of the sorted k dist graph. Fine-tuning was achieved by scanning through 3–6 minimal points and the smallest range of eligible epsilon values, plotting noise points in obtained graphs (custom code Julian Spagnuolo: https://github.com/JulianSpagnuolo/FACkit). tSNE plots were generated with ggplot2[63] and individual marker expression were plotted using the ggbeeswarm package https://github.com/eclarke/ggbeeswarm). Heatmaps were created with pheatmaps package (https://github.com/raivokolde/pheatmap). All graphs were compiled with Affinity Designer 2 (Pantone LLC).

Co-receptor usage prediction

We aligned translated V3 sequences and did co-receptor usage predictions with the online analysis tool geno2pheno with a false positive rate of 10% for CXCR4 detection (https://coreceptor.geno2pheno.org/index.php).

Statistical analysis

All data are presented as median or mean ±SD. All statistical details of the experiments can be found in the results section. Differences were considered statistically significant at $p < 0.05$. FACS data were computed by RStudio (2022.12.0 + 353, Posit Software, PBC). Pearson correlation plots were either generated with Prism (9.5.0, Graphpad Software, LLC) or with raw FACS data using the ggpubr package (https://github.com/kassambara/ggpubr).